Composition and origin of rhyolite melt intersected by drilling in the Krafla geothermal field, Iceland

R. A. Zierenberg, P. Schiffman, G. H. Barfod, C. E. Lesher, N. E. Marks, J. B. Lowenstern, A. K. Mortensen, E. C. Pope, et al.

Contributions to Mineralogy and Petrology

ISSN 0010-7999

Contrib Mineral Petrol
DOI 10.1007/s00410-012-0811-z

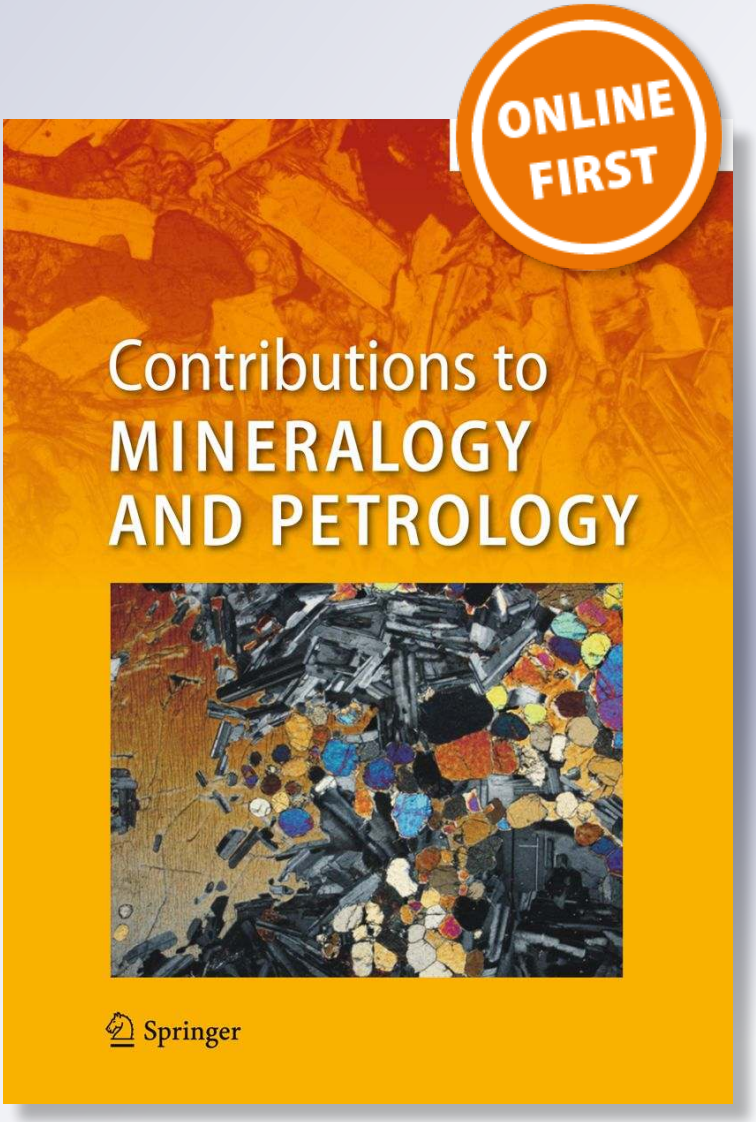

Springer

Your article is protected by copyright and all rights are held exclusively by Springer-Verlag. This e-offprint is for personal use only and shall not be self-archived in electronic repositories. If you wish to self-archive your work, please use the accepted author's version for posting to your own website or your institution's repository. You may further deposit the accepted author's version on a funder's repository at a funder's request, provided it is not made publicly available until 12 months after publication.

Author's personal copy

Contrib Mineral Petrol
DOI 10.1007/s00410-012-0811-z

ORIGINAL PAPER

Composition and origin of rhyolite melt intersected by drilling in the Krafla geothermal field, Iceland

R. A. Zierenberg · P. Schiffman · G. H. Barfod · C. E. Lesher · N. E. Marks · J. B. Lowenstern · A. K. Mortensen · E. C. Pope · D. K. Bird · M. H. Reed · G. Ó. Friðleifsson · W. A. Elders

Received: 31 January 2012 / Accepted: 3 September 2012
© Springer-Verlag 2012

Abstract The Iceland Deep Drilling Project Well 1 was designed as a 4- to 5-km-deep exploration well with the goal of intercepting supercritical hydrothermal fluids in the Krafla geothermal field, Iceland. The well unexpectedly drilled into a high-silica (76.5 % SiO_2) rhyolite melt at approximately 2.1 km. Some of the melt vesiculated while extruding into the drill hole, but most of the recovered cuttings are quenched sparsely phyric, vesicle-poor glass. The phenocryst assemblage is comprised of titanomagnetite, plagioclase, augite, and pigeonite. Compositional zoning in plagioclase and exsolution lamellae in augite and pigeonite record changing crystallization conditions as the melt migrated to its present depth of emplacement. The in situ temperature of the melt is estimated to be between 850 and 920 °C based on two-pyroxene geothermometry and modeling of the crystallization sequence. Volatile content of the glass indicated partial degassing at an in situ pressure that is above hydrostatic ($\sim$16 MPa) and below lithostatic ($\sim$55 MPa). The major element and minor element composition of the melt are consistent with an origin by partial melting of hydrothermally altered basaltic crust at depth, similar to rhyolite erupted within the Krafla Caldera.

Communicated by T. L. Grove.

R. A. Zierenberg (✉) · P. Schiffman · G. H. Barfod · C. E. Lesher · N. E. Marks
Department of Geology, University of California-Davis, Davis, CA 95616, USA
e-mail: razierenberg@ucdavis.edu

Present Address:
N. E. Marks
Lawrence Livermore National Labs, 7000 East Avenue, Livermore, CA 94550, USA

J. B. Lowenstern
U.S. Geological Survey, 345 Middlefield Rd., Menlo Park, CA 94025, USA

A. K. Mortensen
Iceland GeoSurvey (ISOR), Grensásvegur 9, IS 108 Rekjavik, Iceland

E. C. Pope · D. K. Bird
Department of Geological and Environmental Sciences, Stanford University, Stanford, CA 94305, USA

Present Address:
E. C. Pope
Natural History Museum of Denmark, Copenhagen University, Øster Voldgrad 5-7, 1350 København K, Denmark

M. H. Reed
Department of Geological Sciences, 1272 University of Oregon, Eugene, OR 97403, USA

G. Ó. Friðleifsson
HS Orka hf, Brekkustigur 36, IS 260 Reykjanesbær, Iceland

W. A. Elders
Department of Earth Sciences, University of California-Riverside, Riverside, CA 92521, USA

Published online: 22 September 2012

Author's personal copy

Chondrite-normalized REE concentrations show strong light REE enrichment and relative flat patterns with negative Eu anomaly. Strontium isotope values (0.70328) are consistent with mantle-derived melt, but oxygen and hydrogen isotope values are depleted (3.1 and −118 ‰, respectively) relative to mantle values. The hydrogen isotope values overlap those of hydrothermal epidote from rocks altered by the meteoric-water-recharged Krafla geothermal system. The rhyolite melt was emplaced into and has reacted with a felsic intrusive suite that has nearly identical composition. The felsite is composed of quartz, alkali feldspar, plagioclase, titanomagnetite, and augite. Emplacement of the rhyolite magma has resulted in partial melting of the felsite, accompanied locally by partial assimilation. The interstitial melt in the felsite has similar normalized SiO_2 content as the rhyolite melt but is distinguished by higher K_2O and lower CaO and plots near the minimum melt composition in the granite system. Augite in the partially melted felsite has re-equilibrated to more calcic metamorphic compositions. Rare quenched glass fragments containing glomeroporphyritic crystals derived from the felsite show textural evidence for resorption of alkali feldspar and quartz. The glass in these fragments is enriched in SiO_2 relative to the rhyolite melt or the interstitial felsite melt, consistent with the textural evidence for quartz dissolution. The quenching of these melts by drilling fluids at in situ conditions preserves details of the melt–wall rock interaction that would not be readily observed in rocks that had completely crystallized. However, these processes may be recognizable by a combination of textural analysis and in situ analytical techniques that document compositional heterogeneity due to partial melting and local assimilation.

Keywords Krafla · Iceland · Geothermal · Rhyolite · Basalt partial melting · Stable isotope · Strontium isotope

Introduction

The Iceland Deep Drilling Project (IDDP) is an industry–government consortium with the goal of exploring for supercritical hydrothermal fluids that could be utilized for energy production (Friðleifsson and Elders 2005; Friðleifsson et al. 2010; Elders and Friðleifsson 2010). The IDDP-1 drill hole was designed to drill 4–5 km into the Krafla geothermal field, but the hole unexpectedly intersected a rhyolite melt at approximately 2,100 m that prevented further drilling (Elders et al. 2011). Magma has been intersected during geothermal exploration drilling on two previous occasions. A well in the Puna Geothermal field, Hawaii, intersected dacitic melt at 2,488 m depth in 2005 (Teplow et al. 2009). This melt is interpreted as an end-stage differentiate of basaltic magma injected into the Kilauea East Rift zone. Peraluminous, partially hydrated glass ranging in silica content from 69.0 to 78.8 wt% was previously recovered in the Krafla geothermal system in 2008 at a depth of 2,571 m from well KJ-39 drilled into Suðurhliðar well field (Mortensen et al. 2010). This glass was interpreted to have formed in situ by partial melting of hydrated basalt in the contact zone of a gabbroic intrusion (Mortensen et al. 2010). This paper describes the observation of a rhyolite melt generated at depth and emplaced into a sequence of rhyolite intrusives of similar composition. The quenched glasses recovered in the drill cuttings provide the first opportunity to observe details of the in situ interaction of a rhyolite intrusion with its wall rocks, including partial melting and assimilation, processes that would be difficult to constrain in a completely crystallized sequence of rhyolite intrusions.

Geologic setting

The Krafla central volcano is located on the North Iceland Rift Zone (Fig. 1). The Krafla geothermal field is located in a large (∼8 km) collapse caldera that formed approximately 110 ka (Sæmundsson 1991). The caldera is bisected by the NNE–SSW fissure swarm that marks the North Iceland Rift Zone. The caldera is largely filled by basaltic lavas and hyaloclastites. Rhyolite has erupted periodically, but intermediate composition lavas are not abundant (Sæmundsson 1991; Jónasson 1994). The caldera has been the site of extensive drilling for geothermal development since 1974, which reveals the extent of several active geothermal systems and defines the subsurface geology (Kristmannsdóttir 1978; Stefánsson 1980, 1981; Ármannsson et al. 1987). The near-surface, postglacial basaltic lavas are underlain by hyaloclastite erupted during the last glacial stage (Guðmundsson 1983). A second, older sequence of hyaloclastite is overlain and underlain by interglacial lavas down to about ∼1,200 m, where intrusive rocks begin to dominate. Doleritic intrusions are abundant in the deeper parts of the reservoir, but felsic intrusions have been intersected in several drill holes (Guðmundsson 1983; Ármannsson et al. 1987). Intrusions become more abundant and coarser grained at greater depth and include gabbros, especially in the Suðurhliðar well field.

A prograde hydrothermal alteration assemblage is developed with depth, and the epidote–actinolite zone (>280 °C) is encountered at shallowest depths beneath the Suðurhliðar well field where the geothermal fluid temperatures are controlled by the depth to boiling (Ármannsson et al. 1987; Arnórsson et al. 2008). In the Leirbotnar well field, where IDDP-1 was drilled, the geothermal system is divided into an upper reservoir that is sub-boiling (∼190–220 °C), separated by a relatively impermeable

Author's personal copy

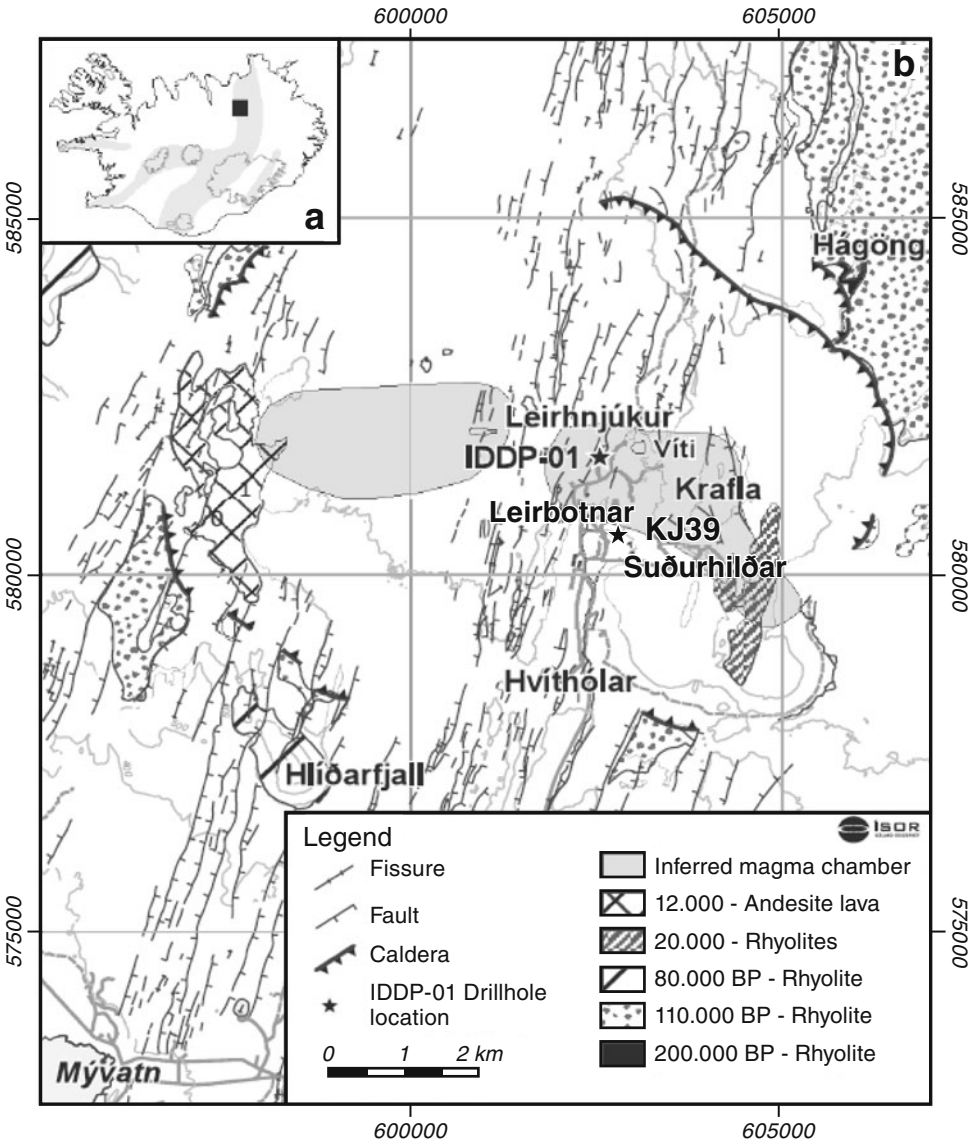

Fig. 1 Location of the Krafla geothermal field on the North Iceland Rift Zone is shown in the inset map (**a**). Map of the Krafla caldera (**b**) showing the location of IDDP-1 and KJ-39 drill holes, the extent of felsic rocks, and the surface projection of subsurface melt (modified from Sæmundsson 2008)

zone from a lower high-temperature (~280–340 °C) fluid and steam reservoir (Stefánsson 1981; Böðvarsson et al. 1984; Ármannsson et al. 1987). Fluid temperatures in the lower reservoir are generally controlled by depth to boiling, but superheated steam has been encountered in some wells (Guðmundsson et al. 2008; Einarsson et al. 2010). Geothermal fluids produced are generally low salinity, neutral chloride fluids recharged by meteoric waters (Ármannsson et al. 1987; Arnórsson et al. 2008; Ármannsson 2010), but some wells are acidic due to input of magmatic volatiles, which increased greatly in the Leirbotnar well field during the Krafla Fires (Ármannsson et al. 1989).

The most recent eruption in this area was the Krafla Fires and rifting episode that initiated with basaltic fissure eruptions in 1975 and continued intermittently until 1984. A similar event, known as the Mývatn Fires, occurred from 1724 to 1729. The Mývatn Fires basaltic fissure eruption was immediately preceded by a phreatomagmatic eruption that formed the Viti crater (Fig. 1), which produced very minor amounts of juvenile rhyolitic pumice and basaltic scoria (Sæmundsson 1991; Jónasson 1994). The youngest rhyolitic eruption is the Hveragil tephra erupted about 9,000 BP (Sæmundsson 1991).

The IDDP-1 well was engineered and cased to drill to depths of 4–5 km with the intention of intersecting and producing geothermal fluid under supercritical conditions (>374 °C at >22.1 MPa for pure water). The hole was sited based on the data derived from 39 drill holes and numerous geophysical and geochemical studies conducted in the Krafla area over the last three decades. A magma body is inferred to underlie Krafla Caldera at depths of 3–7 km based on observation of attenuation of S-waves during the Krafla Fires rifting episode (Fig. 1; Einarsson 1978). A recent transient-electromagnetic-magnetotelluric (TEM-MT) survey delineated a

Author's personal copy

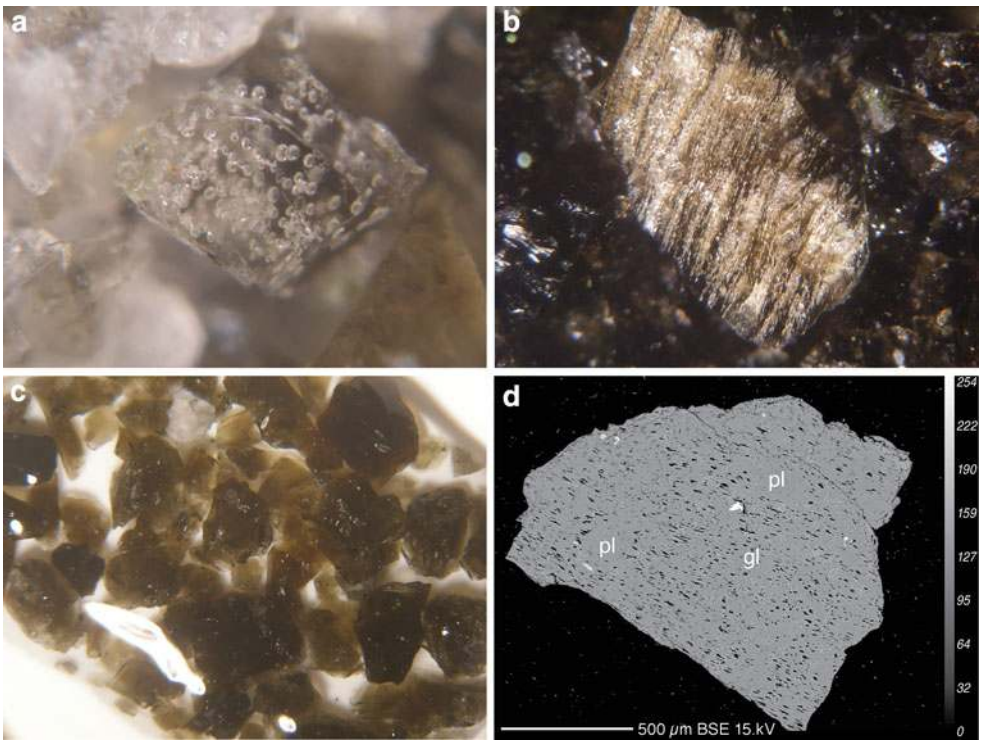

Fig. 2 Rhyolite glass cuttings from IDDP-1. **a** Vesiculated clear volcanic glass quenched from Melt-1; grain size is approximately 1 mm. **b** Stretched bubble pumice quenched from Melt-1; grain size is approximately 1 mm. **c** Typical poorly vesiculated, sparsely phyric rhyolite glass quenched from Melt-1; average grain size approximately 2 mm. **d** BSE image of stretched bubble pumice with phenocrysts of plagioclase (pl) and titanomagnetite (*bright*) in Melt-1 glass (gl)

deep conductor that might represent the brittle–ductile boundary at the top of a melt zone, and IDDP-1 was sited to drill between, but not intersect, two shallow lobes that extended to less than 3 km depth elsewhere in the field (Elders et al. 2011, Figure DR1 in GSA Data Repository 2011088).

Drilling into the melt

Loss of circulation and stuck drill strings required cementation at the bottom of the initial hole (IDDP-1) and eventually led to two sidetrack drilling attempts (IDDP-1B,C) (Hólmgeirsson et al. 2010). Loss of circulation due to intersection of a high permeability zone was encountered in each of the three drilling tracks in Hole IDDP-1 at depths near 2,100 m, followed by drilling difficulties, including high torque and stuck drill strings. Loss of circulation in the final offset hole, IDDP-1C, resulted in no cutting returns from deeper than 2,070 m. A sudden increase in the rate of penetration at 2,104.4 m was followed by an increase in torque, and the drill string was raised with some difficulty several meters (Hólmgeirsson et al. 2010). When the drill string was lowered again it became stuck 9.3 m above the bottom of the hole and the standpipe pressure spiked to 180 bars. Following this, cuttings fragments were again returned to the surface, initially in pulsed flow. The initial cuttings were clear vesiculated volcanic glass (Fig. 2a) quenched from melt by the down hole circulation of drilling water. Fragments of stretched bubble pumice (Fig. 2b) indicate the melt was extruding into the hole. After about 1.5 h, the dominant fragments returned to the surface were dark brown sparsely phyric glass shards (Fig. 2c), interpreted to have formed by subsurface phreatomagmatic explosive interaction with the drilling water. Felsic intrusive fragments, some showing quenched melt pockets, were also recovered. Cutting analysis and high natural gamma counts in the down hole log indicated that the melt was emplaced into crystalline felsic intrusive rocks (Gautason et al. 2010).

Methods

Two types of material were available for study, drill cuttings (typically <4 mm) and bulk rock fragments (>1 cm), and the techniques employed were dependent on the nature of the material.

Author's personal copy

Drill cuttings

Drill cuttings were collected at the drill rig. Although drilling advance stopped when rhyolite melt was encountered at 2,104.4 m, cuttings continued to be carried to the drill floor by circulating cooling water through the drill string, and cuttings were collected and archived as a time series at approximately 15-min intervals. Polished sections of the cuttings were examined by reflected light microscopy and using backscattered electron (BSE) imaging, coupled with energy dispersive spectroscopy, on a Cameca SX-100 electron microprobe (EMP) equipped with 5 wavelength dispersive spectrometers.

Quantitative EMP analyses were performed at 15 keV and using spot sizes/beam currents of 10 μm/5 nA for rhyolite glass, 5 μm/10 nA for feldspars, and 1 μm/10 nA for pyroxenes. The following silicate and oxide standards were used in conjunction with conventional ZAF matrix corrections, for glass: corning synthetic glass GSC (Na, Mg, Al, K, Ca, and Fe), RLS 132 rhyolite glass (Si), TiO_2 (Ti), and rhodonite (Mn); for pyroxene: omphacite (Na), tremolite (Mg), augite (Al, Si, Ca), TiO_2 (Ti), rhodonite (Mn), and fayalite (Fe); and for feldspar: orthoclase (K), albite (Na, Si, Al), haematite (Fe), and wollastonite (Ca). Each analyte line and its corresponding background were measured for 10 s, except for Si, K, and Ca on glasses, which were measured for 20 s on both peak and background. Data presented in Table 1 are averages of from 1 to 8 points on individual cutting fragments. Elemental plots are normalized to 100 % (anhydrous) for comparison between glasses.

Samples of clear vesiculated glass and dark vesicle-poor glass were separated by hand picking under a binocular microscope and analyzed for volatile content by Fourier Transform Inferred spectroscopy (FTIR) at the USGS in Menlo Park using the absorption coefficients and methods described in Lowenstern et al. (1997) and Elders et al. (2011). Hand-picked separates of clear vesiculated glass

Table 1 Major element composition of glass (wt%), determined by electron microprobe, and whole rock, determined by X-ray fluorescence

	Na_2O	MgO	Al_2O_3	SiO_2	K_2O	CaO	TiO_2	MnO	FeO	P_2O_5	Anhydrous total	H_2O	CO_2	Total
Melt-1														
7-A(8)	3.75	0.16	11.72	75.42	3.05	1.21	0.30	0.05	2.58	n.a	98.25			
7-E(4)	3.76	0.19	11.77	74.74	2.94	1.35	0.34	0.09	2.72	n.a	97.90			
7-HH(6)	3.71	0.20	11.90	75.07	2.91	1.40	0.35	0.05	2.85	n.a	98.43			
28-R(5)	3.76	0.24	11.88	74.41	2.96	1.49	0.34	0.08	2.84	n.a	97.99			
1700-R(6)	3.60	0.15	11.67	75.29	3.10	1.17	0.27	0.06	2.50	n.a	97.80			
Average	3.72	0.19	11.79	74.99	2.99	1.32	0.32	0.07	2.70	n.a	98.07	1.77	0.0085	99.85
Anhydrous normalized	3.79	0.19	12.02	76.47	3.05	1.35	0.33	0.07	2.75	n.a	100.00			
Melt-2														
7-K(5)	3.47	0.06	11.77	76.11	5.07	0.47	0.25	0.05	1.56	n.a	98.80			
28-G(6)	3.54	0.06	11.76	75.15	5.04	0.52	0.20	0.11	1.77	n.a	98.15			
1700-G1a(4)	3.46	0.07	11.72	75.69	5.18	0.47	0.13	0.09	1.84	n.a	98.65			
1700-G1b(6)	3.65	0.07	11.76	75.87	5.11	0.47	0.15	0.11	1.85	n.a	99.05			
1700-G2a(3)	3.56	0.06	11.73	76.27	5.02	0.48	0.21	0.07	1.75	n.a	99.15			
1700-G2b(1)	3.31	0.08	11.94	76.26	5.59	0.47	0.23	0.01	2.00	n.a	99.89			
Average	3.52	0.07	11.57	76.29	4.98	0.48	0.21	0.09	1.82	n.a	99.03			
Anhydrous normalized	3.55	0.07	11.68	77.04	5.03	0.48	0.21	0.09	1.84	n.a	100.00			
Melt-3														
7-CC(6)	3.56	0.10	11.49	76.40	3.84	0.70	0.19	0.05	1.88	n.a	98.20			
7-VN(5)	3.53	0.10	11.54	76.48	4.06	0.68	0.22	0.04	1.77	n.a	98.42			
1700-ZP(3)	3.47	0.09	11.44	76.57	3.91	0.75	0.20	nd	1.83	n.a	98.24			
Average	3.52	0.10	11.49	76.48	3.94	0.71	0.20	0.02	1.82	n.a	98.29			
Anhydrous normalized	3.58	0.10	11.69	77.81	4.01	0.72	0.20	0.02	1.85	n.a	100.00			

JB-2	Na_2O	MgO	Al_2O_3	SiO_2	K_2O	CaO	TiO_2	MnO	FeO	P_2O_5	Total	LOI	
Felsite													
	4.00	0.35	11.86	74.93	2.72	1.65	0.42	0.07	2.96	0.07	99.03	0.23	99.26
Anhydrous normalized	4.04	0.35	11.98	75.66	2.75	1.67	0.42	0.07	2.99	0.07	100.00	0.23	

n.a. not analyzed

Author's personal copy

and dark vesicle-poor glass were analyzed for $\delta^{18}O$ and δD at Stanford University using the methods described in Elders et al. (2011).

Approximately 100 mg samples of dark rhyolite glass and melt-bearing-felsite cuttings were separated under a binocular microscope and prepared for inductively coupled plasma mass spectrometry (ICP-MS) analysis. Samples for trace element analysis were digested in closed Savillex® PFA containers in concentrated HF-HNO_3, and trace elements were determined on an Agilent 7500ce ICP-MS at UC Davis. USGS diabase W-2 working standard was analyzed using the same procedures, and all values were within 17 % of the recommended values. For strontium isotope analyses, about 50 mg was weighed out, digested in closed Savillex® PFA containers in concentrated HF-HNO_3, and loaded in 8 N HNO_3 on Teflon microcolumns containing Eichrom Sr Spec resin. Strontium was eluted by 0.1 N HNO_3 following rinses by 3 N HNO_3 to remove matrix and interfering elements including Rb, Ba, and Pb. After dry-down, the procedure was repeated to ensure complete purification of Sr from Rb. Samples were introduced to the Nu Plasma (Nu032) multi-collector inductively coupled plasma mass spectrometer (MC-ICP-MS) at the UC Davis Interdisciplinary Center for Plasma Mass Spectrometry with a desolvating nebulizer (DSN-100). Sr isotopic ratios were corrected for mass fractionation to $^{86}Sr/^{88}Sr = 0.1194$. ^{87}Rb was monitored to correct for the interference of ^{86}Rb on ^{86}Sr. $^{87}Sr/^{86}Sr$ isotope ratios for the samples were normalized to an accepted value of 0.710248 for the SRM 987 standard. Repeat analysis of SRM 987 gives an uncertainty of ± 0.000011 (2σ, $n = 12$). Normalized $^{87}Sr/^{86}Sr$ ratios of 0.705041 (± 0.000013) and 0.708296 (± 0.00023) were obtained for standards USGS standards BCR-2 and G-2, respectively.

Rhyolite glass and glass quenched from interstitial melt pockets in felsite were also analyzed for a suite of trace elements, using laser ablation inductively coupled mass spectrometry (LA-ICP-MS) at the UC Davis Interdisciplinary Center for Plasma Mass Spectrometry. A New Wave Research UP-213-nm laser ablation systems was used to ablate 50- to 80-μm spots in a He atmosphere, and the aerosol was analyzed using a Agilent Technologies 7500a quadrupole ICP-MS. NIST glass 610 was used as the calibration standard with NIST glass 612 as a control standard. Calcium was used as an internal standard for LA-ICP-MS by normalizing ^{43}Ca counts to match the CaO concentration determined on the sample glasses by electron microprobe.

Rock fragments

Several larger fragments of rock, up to 5 cm across, were collected in a junk basket following a milling run at 2,042.7 m in Hole IDDP-1B prior to drilling into the rhyolite melt. These samples do not retain any stratigraphic continuity, but comparison to the cuttings indicates that the lithologies recovered are similar to the lithologies penetrated below ~2,000 m. Several fragments were observed in thin section. Most of the larger felsic rock fragments are mineralogically and texturally similar to the felsite cuttings derived from the wall rocks of the rhyolite magma. A sample of felsite (JB-2) that showed the same mineral assemblage as the felsite cuttings from deeper in the hole was analyzed for major elements using XRF and trace elements using ICP-MS at the Washington State University GeoAnalytical Laboratory, using procedures described in Marks et al. (2009).

Results

Petrography of the glasses and their host rocks

Three high-silica rhyolite glasses quenched from melt by the drilling fluid have been identified based on their petrography, as detailed below.

Melt-1

The dominant cuttings fragments recovered from the bottom of IDDP-1C are sparsely phyric (<3 % crystals), dark brown, poorly vesiculated, rhyolite glass with a refractive index of 1.490 (Fig. 2c). White, sparsely phyric pumiceous glass fragments were most abundant in the initial cutting returns, and some of these show highly stretched bubbles (Fig. 2b, d). The vesiculated cuttings fragments have refractive index and phenocrysts assemblages identical to the brown glass cuttings. White vesiculated pumice has been observed interbanded with dark brown glass. Fine-grained (0.1–1 mm), subhedral titanomagnetite microphenocrysts are ubiquitous in the glass (Fig. 3a). Rarely, they contain rounded inclusions of pyrrhotite, which also occurs as round blebs in the glass. Prismatic crystals of green pigeonite up to a few mm long co-exist with smaller, equant, brownish-yellow/green clinopyroxene. Although many crystals show some well-developed crystal faces, textures indicative of dissolution/resorption are also present (Fig. 3b). Both pigeonite and augite commonly show exsolution lamellae of the alternate phase, often in more than one orientation (Fig. 3c). Augite overgrowths are present on some pigeonites (Fig. 3d). Euhedral plagioclase is present in approximately the same abundance as pyroxene. Trace amounts of microphenocrysts (~10 μm) of apatite are present, typically as inclusions in plagioclase. Quartz crystals are not present in glass quenched from Melt-1.

Author's personal copy

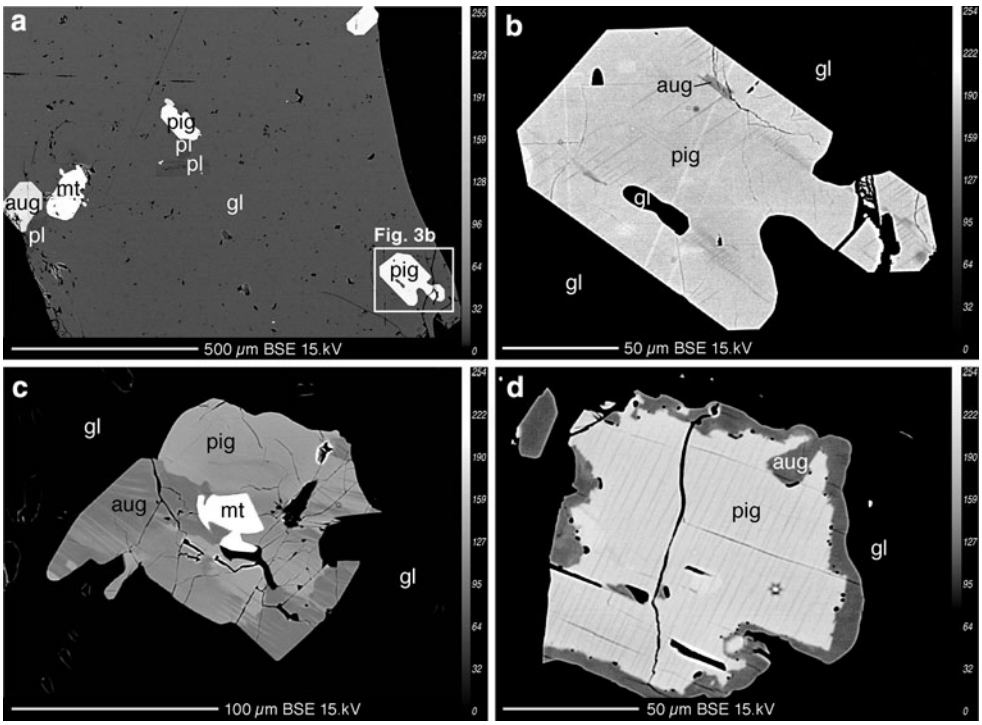

Fig. 3 Back scattered electron (BSE) images. **a** Typical, poorly vesiculated sparsely phyric Melt-1 glass (gl) with phenocrysts of plagioclase (pl), titanomagnetite (mt), pigeonite (pig), and augite (aug). **b** Pigeonite phenocrysts with darker exsolution lamellae of augite. **c** Intergrown augite and pigeonite with exsolution lamellae of the alternate phase. **d** Pigeonite phenocrysts with fine darker exsolution lamellae of augite and a later rim of augite overgrowing the pigeonite

Melt-2

Cutting fragments of crystalline felsic intrusive rock recovered with the quenched rhyolite glass are representative of the host rock into which the rhyolite melt was emplaced. The felsite is composed of 0.1- to 1-mm alkali feldspar, plagioclase, quartz, titanomagnetite, and augite (Fig. 4a). Rare fragments have co-existing high-K and low-K alkali feldspar phenocrysts, but lack plagioclase. Anhedral quartz is abundant, as are anhedral to rounded magnetite grains. Subhedral augite is present and shows irregular zoning/intergrowths as indicated by backscatter intensity, but relatively minor variations in composition. Small apatite crystals are common, and rare zircon grains up to 40 μm in long dimension were observed.

Quenched rhyolite glass of Melt-2 occurs in variable amounts (up to ~20 %) interstitial to the mineral phases in most felsite cutting grains. In one fragment only, we found evidence for very local hydration of the glass, which we interpret to have occurred by reaction with the drilling fluids after the glass was quenched by the drilling fluid. Although this hydrated glass is present in only trivial amounts, we describe it here because of the unexpected rapidity at which it must have formed. The hydrated glass is distinguished by lower backscatter intensity and can be seen as <5-μm-wide reaction rims on vesicles and in glass present in thin segregations and cracks in alkali feldspar. The hydrated glass generally occurs adjacent to open fractures in fresh glass. Microprobe analysis of the hydrated glass shows that the cation ratios are identical to the fresh glass but that anhydrous oxide totals range from 93.1 to 94.2 %, compared with 98.7 % for the fresh glass (Table 1).

Melt-3

Some glass fragments contain abundant crystals and/or glomerocrysts of quartz, plagioclase, augite, and magnetite (Fig. 4b) that are texturally and mineralogically similar to the felsite, except they typically lack alkali feldspar or contain small irregular grains of residual alkali feldspar. Some plagioclase grains show irregular compositional zoning that locally appears to record partial resorption of the crystals (Fig. 4c). Quartz in these crystal-rich areas is typically highly embayed and appears to be undergoing resorption (Fig. 4d). The glass in these crystal-rich fragments is typically moderately vesiculated, and vesicle elongation preserves the pattern of melt flow around the crystal aggregates. The textures suggest invasion and partial assimilation of the felsite by the rhyolite melt. Glass analyses from these rare crystal-rich fragments plot between the fields defined by the rhyolite glass and the

Author's personal copy

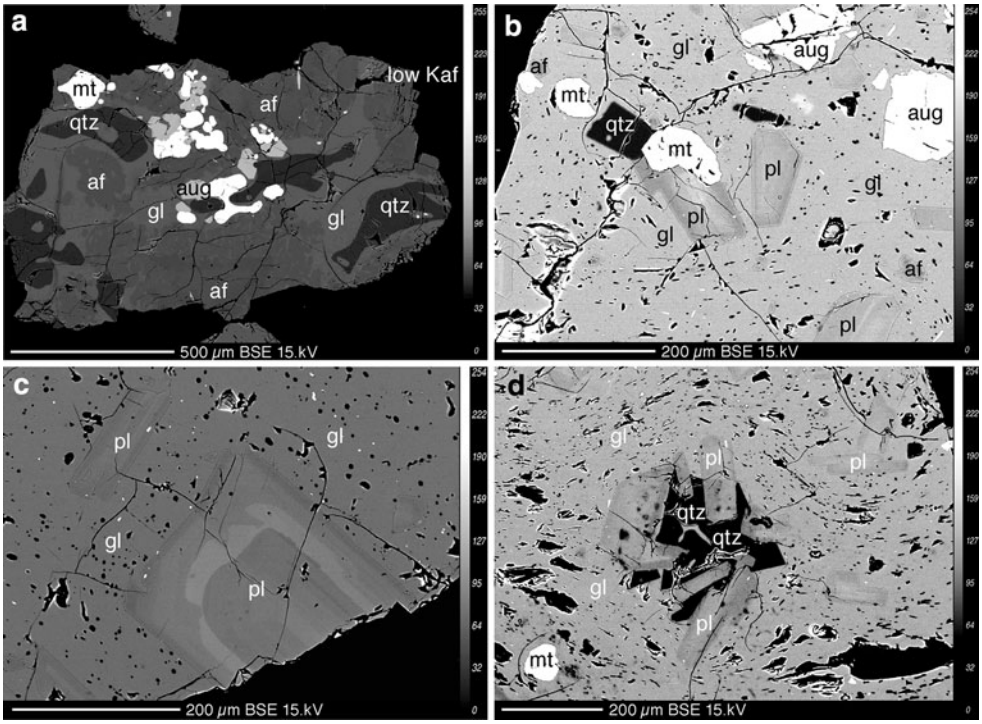

Fig. 4 BSE images. **a** Felsite showing rounded phenocryst of titanomagnetite (mt), augite (aug), partially resorbed alkali feldspar (af), lower-K ternary alkali feldspar (low-K af), and partially resorbed quartz (qtz), with patches of interstitial Melt-2 quenched to glass (gl). **b** Partially assimilated felsite with quartz, augite, titanomagnetite, and plagioclase in Melt-3 glass. **c** Zoned plagioclase phenocrysts in Melt-3 glass. Brighter backscatter in the plagioclase indicates higher anorthite content. **d** Partially assimilated felsite with titanomagnetite, and glomerocrysts of plagioclase (pl-rectangular) and partially resorbed quartz (qtz-dark). Note the lack of alkali feldspar and the flow of melt around the glomerocrysts defined by the elongate vesicles

quenched interstitial glass in the felsite, as discussed below.

Chemistry

Glass composition

Electron microprobe analyses show that both Melt-1 and Melt-2 are high-silica rhyolites (Table 1). The major difference in the glass compositions is the higher K and lower Ca content of the Melt-2. CIPW normative composition of Melt-2 plots near the low-pressure minimum melting composition in the albite–orthoclase–quartz system (Fig. 5). The composition of Melt-1 is similar to a whole-rock sample of crystalline felsite (JB-2) analyzed by XRF (Table 1). The glomerophyric, crystal-rich glass fragments quenched from Melt-3 lie between Melt-1 and Melt-2 on a plot of Na_2O versus K_2O (Fig. 6a) or K_2O versus CaO (Fig. 6b), suggesting mixing of the two melts. However, plots of K_2O versus SiO_2 (Fig. 6c) and CaO versus SiO_2 (Fig. 6d) show excess silica compared with the other two melts, consistent with the textural evidence for resorption of quartz.

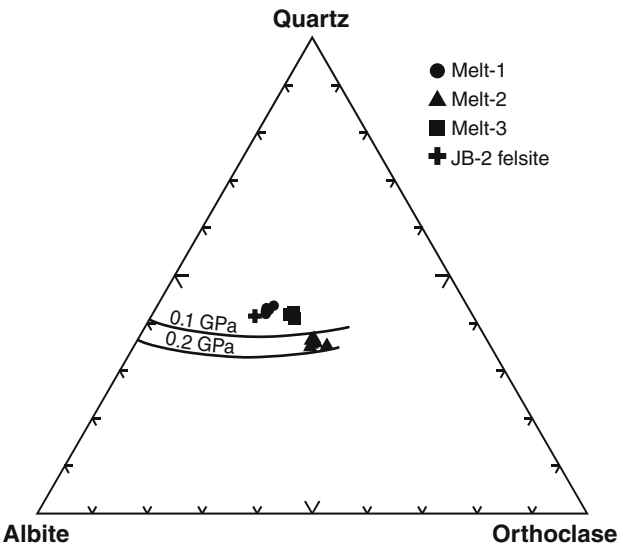

Fig. 5 CIPW normative compositions of Melt-1 rhyolite glass are very similar to a sample of crystalline felsite (JB-2). Interstitial partial melt in felsite, Melt-2, plot between the 0.1 and 0.2 GPa cotectic curves for minimum melting in the system albite–orthoclase–quartz presented in Winter (2001). Melt-3 plots at intermediate composition

Chondrite-normalized (Sun and McDonough 1989) REE plots of hand-picked Melt-1 glass cuttings, felsite cuttings with interstitial glass quenched from Melt-2,

Author's personal copy

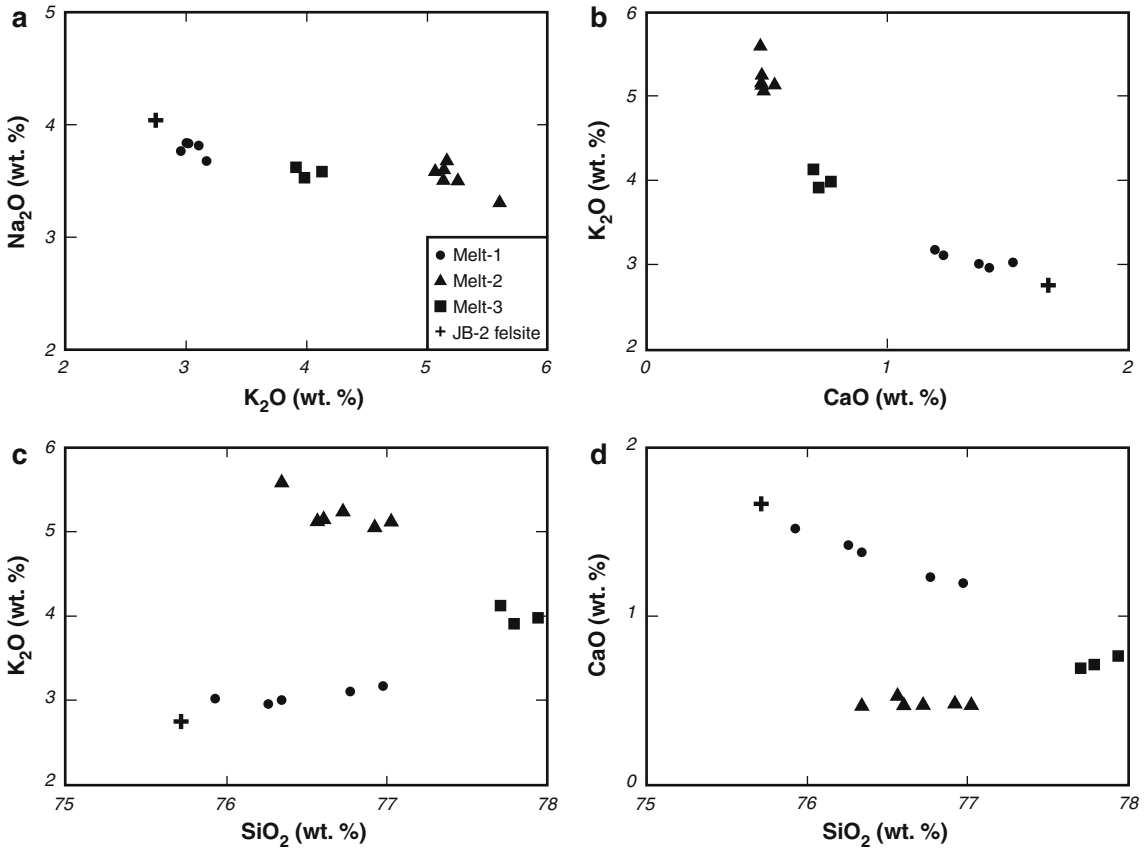

Fig. 6 Chemical variation diagrams for crystalline felsite (JB-2) and the different glasses; data normalized to anhydrous compositions. **a** K_2O versus Na_2O. **b** CaO versus K_2O. **c** SiO_2 versus K_2O. **d** SiO_2 versus CaO

and a sample of crystalline felsite (JB-2) all show nearly identical REE concentrations and REE patterns characterized by light REE enrichment and negative europium anomalies (Fig. 7a, Table 2). Laser Ablation ICP-MS analysis was used to compare the whole-rock dissolution data to in situ analysis of Melt-1 glass and the interstitial melt in the felsite (Melt-2), which could not be physically separated from its crystalline matrix (Table 3). Only the more abundant, even-numbered REE were analyzed, but comparison of the LA-ICP-MS data and the solution data for the Melt-1 glass show that the LA-ICP-MS data overlap the solution data (Fig. 7a). The Melt-2 glass is highly enriched in REE relative to the bulk sample of the felsite with enrichment factors of 6.0 for La decreasing to 4.6 for Sm and Gd and increasing again to 6.0 for Yb. Trace element patterns, normalized to NMORB (Sun and McDonough 1989), are very similar for Melt-1 and the felsite (JB-2) (Fig. 7b). LA-ICP-MS data mimic the solution data and show that Melt-2 glass is enriched in most trace elements relative to JB-2. The Melt-2 glass shows a more pronounced depletion in Sr and a strong depletion in Ba relative to JB-2.

Melt-1 glass cuttings and the Melt-2-bearing felsite cuttings have $^{87}Sr/^{86}Sr$ isotope ratios 0.703280 and 0.703323, respectively, and these values are similar to mantle-derived basalts from the north Iceland rift (Moorbath and Walker 1965; Sigmarsson et al. 1991, 1992).

Samples of brown, poorly vesiculated Melt-1 glass, clear vesiculated Melt-1 glass, and white pumiceous Melt-1 glass were analyzed for volatile content using FTIR (Table 4). The volatile contents of the samples overlap with no distinguishable difference based on color or texture. The average total water content is 1.77 wt% (±0.14) (Fig. 8), consistent with the electron microprobe totals (Table 1). Average CO_2 content is 85 ppm (±15). Clear vesiculated Melt-1 glass and the typical dark brown Melt-1 glass also have identical oxygen and hydrogen isotope ratios with $\delta^{18}O = 3.2$ ‰ and $\delta D = -118$ ‰, values that are isotopically depleted in the heavier isotope relative to mantle-derived melts (Eiler 2001).

Mineral chemistry

The compositions of pyroxenes determined by electron microprobe (Table 5) are shown in Fig. 9. Spot analyses

Author's personal copy

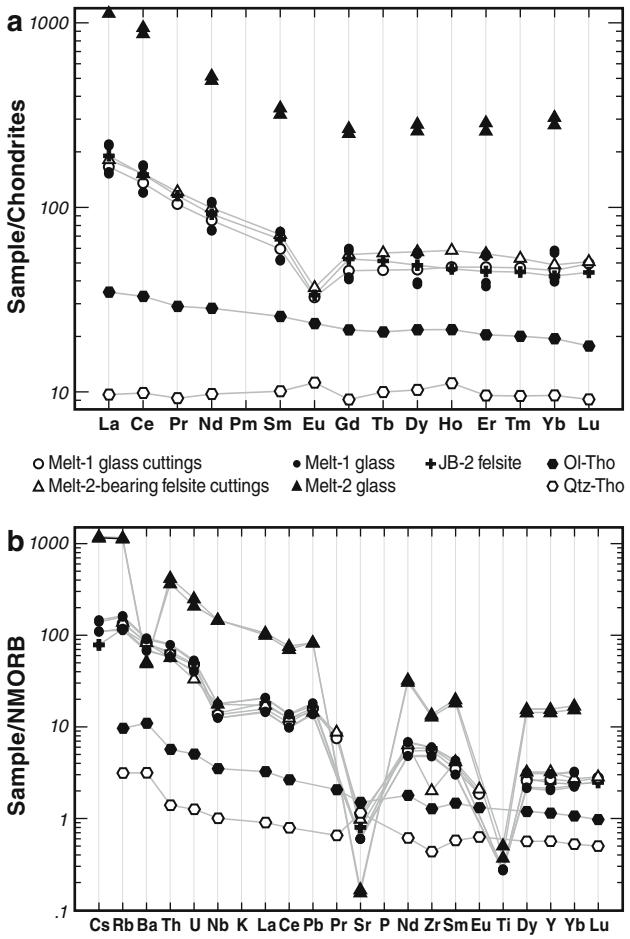

Fig. 7 Trace element data for hand-picked Melt-1 glass cuttings (*open circles*), hand-picked Melt-2-bearing felsite cuttings (*open triangles*) and JB-2 felsite (*plus*) determined by ICP-MS. In situ spot analyses of even-numbered REE determine by LA-ICP-MS on Melt-1 glass (*filled circles*) and Melt-2 glass in felsite (*filled triangles*). **a** Chondrite-normalized (Sun and McDonough 1989) REE plot. **b** Trace element compositions, normalized to NMORB (Sun and McDonough 1989), for bulk samples (*filled symbols*) of Melt-1 glass cuttings, Melt-2-bearing felsite cuttings, and JB-2 felsite determined by ICP-MS. In situ analysis of Melt-1 glass and Melt-2 glass determined by LA-ICP-MS (*open symbols*). Data from a Krafla olivine tholeiite (*open hexagons*) and a quartz tholeiite (*filled hexagons*) reported in Jónasson (1994) are shown for reference

that fall between pigeonite and augite may represent unexsolved pyroxene but are more likely due to probe spots that overlap the finely intergrown exsolution lamellae and sample both minerals. Pigeonite is more iron-rich than coexisting augite in the Melt-1 glass (Fig. 10) but contains lower Al_2O_3, TiO_2, and Na_2O (Table 5). Augite is the only pyroxene observed in the felsite and has considerably more CaO, MnO, and Na_2O relative to augite in Melt-1 glass (Table 5).

Most plagioclase compositions (Table 6) in Melt-1 glass are andesine in the range from An_{43} to An_{48} (Fig. 11), but some show more extensive compositional zoning. Plagioclase in the Melt-2-bearing felsite is enriched in Na_2O and K_2O compared with plagioclase in the Melt-1 glass (Fig. 11). Alkali feldspar in the felsite also shows a limited range in Na_2O and K_2O. In some cuttings, alkali feldspar is intergrown with anorthoclase (Fig. 11). Plagioclase in the Melt-3 glass cuttings has an overlapping, but somewhat larger range in composition (An_{39} to An_{58}) than Melt-1 and the Melt-2-bearing felsite.

Discussion

Origin of the rhyolite

Bimodal volcanism and the origin of rhyolites associated with the Krafla Caldera have been discussed by several authors, notably Sæmundsson (1978), Ármannsson et al. (1987), Nicholson et al. (1991), Jónasson (1994, 2007). Nicholson et al. (1991) used rock compositions from Krafla and the adjacent Heidarspordur rift segment in a fractional crystallization-crustal assimilation model to explain the origin of rhyolite. They argue that thorium- and oxygen-isotopic data indicate incorporation of hydrothermally altered wall rock during fractional crystallization. Jónasson (1994) analyzed basalts and rhyolites of differing age at Krafla. Melt-1 and the felsite analyzed here are most similar to the phase 3 rhyolites of Jónasson (1994) that erupted during the last glaciation. Compared with the phase 3 rhyolites, our samples extend to slightly higher silica contents but have nearly identical major element. REE and trace element data for phase 3 Krafla rhyolite presented in Jónasson (1994) are not shown on Fig. 7, but they essentially overlap the data from the IDDP-1 rhyolite. Data from a quartz tholeiite, considered as typical of Krafla basalts by Jónasson (1994), are plotted on Fig. 7 for comparison, along with data from an olivine tholeiite considered to be representative of primitive mantle melts at Krafla (Jónasson 1994). The strontium and oxygen isotope ratios of the IDDP-1 rhyolites also overlap those reported for Krafla rhyolite (Jónasson 1994).

Based on multiple lines of evidence, Jónasson (1994) argues that the Krafla rhyolites form by small degrees (<25 %) of partial melting of hydrothermally altered crustal rocks. Our data on the Melt-1 rhyolite glass are consistent with this interpretation. The major element data from Melt-1 glass and the JB-2 felsite have higher normative quartz and albite compared with the Melt-2 glass, which plots near the low-pressure minimum melting cotectic in the granite system (Fig. 5). Spulber and Rutherford (1983) conducted melting experiments using hydrothermally altered basalt as starting material. Their experiments were conducted under water-saturated conditions with amphibole stable and produced melts that were

Author's personal copy

Table 2 Trace element composition of cuttings determined by ICP-MS and of whole rock determined by ICP-MS and XRF (mg/kg)

	Cuttings		Whole rock	
	Melt-1 glass	Melt-2-bearing felsite	JB-2 ICP-MS	JB-2 XRF
Sc	6.57	4.78	9.10	8.00
V	12.33	2.20		5.00
Cr	5.84	4.62		7.00
Co	1.16	n.d.		
Ni	5.98	5.01		7.00
Cu				19.00
Zn	95.94	101.02		63.00
Ga				17.00
Rb	75.65	77.36	65.50	65.00
Sr	99.34	87.92	72.00	72.00
Y	75.14	90.11	68.93	73.00
Zr	410.34	148.07		418.00
Nb	31.66	41.16	33.02	34.10
Cs			0.55	
Ba	527.19	522.76	506.00	505.00
La	39.34	42.96	45.16	47.00
Ce	82.89	93.13	92.37	92.00
Pr	9.91	11.53	11.01	
Nd	39.73	46.41	42.95	43.00
Sm	9.11	10.91	10.28	
Eu	1.89	2.13	1.94	
Gd	9.34	11.42	10.80	
Tb	1.71	2.12	1.92	
Dy	11.69	14.59	12.36	
Ho	2.69	3.31	2.63	
Er	7.85	9.28	7.45	
Tm	1.20	1.35	1.14	
Yb	7.74	8.30	7.22	
Lu	1.26	1.29	1.13	
Hf	10.52	4.48	11.27	
Ta	2.30	2.83	2.57	
W	1.15	0.97		
Pb	4.71	4.32	4.82	6.00
Th	7.46	6.83	7.93	8.00
U	2.23	1.56	2.29	4.00
$^{87}Sr/^{86}Sr$	0.703280	0.703323		
$\delta^{18}O$	3.1 ‰			
δD	−118 ‰			

Blank not analyzed, *n.d.* not detected

less silicic than the Krafla rhyolites. Thy et al. (1990) show that dehydration partial melting of hydrothermally altered basalts at water-undersaturated conditions (P_{H2O} less than 100 MPa) produced melts similar to Icelandic rhyolites. The residuum from partial melting was anhydrous plagioclase-rich pyroxene granulite. Two-pyroxene hornfels altered cuttings do occur together with the rhyolite glass cuttings from well IDDP-1 (Schiffman et al. in review), but textural evidence for partial melting is not observed. France et al. (2010) conducted dehydration partial melting experiments using hydrothermally altered sheeted dikes as starting material. The experiment with the lowest degree of partial melting produced the most silicic melt (72.6 % SiO_2), which has cation ratios similar to that of Melt-1. The light REE enrichment and relatively flat heavy REE patterns for Melt-1 (Fig. 7a) are interpreted to reflect control by clinopyroxene in the source region, and the negative anomalies in Ba, Sr, and Eu indicate control by plagioclase (Jónasson 1994). Brophy (2009) argued that trends of increasing La and Yb with increasing SiO_2 support fractional crystallization as the dominant mechanism for formation of Icelandic rhyolites. The La and Yb concentrations for both Melt-1 and Melt-2 plot below the trend shown by Brophy (2009) for volcanic rocks formed with the rift zone. A fractional crystallization model for these melts is also not compatible with the oxygen and hydrogen isotope composition of the melts. Although the strontium isotope values of Melt-1 overlap those of Krafla basalt (Nicholson et al. 1991; Sigmarsson et al. 1991; Hémond et al. 1993), the oxygen isotope value is depleted relative to mantle-derived melts or basaltic rocks from Krafla, consistent with source rocks that were hydrothermally altered by isotopically light meteoric water (Nicholson et al. 1991; Elders et al. 2011; Pope et al., in review). The chemical composition and stable isotope ratios of the melt are consistent with partial melting of hydrothermally altered basaltic rocks as the source for the Melt-1 rhyolite.

The origin of low $\delta^{18}O$ volcanic rocks derived from the Iceland hot spot has been investigated in several previous studies (Harmon and Hoefs 1995; Skovgaard et al. 2001; Thirlwall et al. 2006; Rose-Koga and Sigmarsson 2008), and many authors have pointed to the role of hydrothermally altered crust as a source of ^{18}O depleted silicic melts (Muehlenbachs et al. 1974; Hattori and Muehlenbachs 1982; Condomines et al. 1983; Hémond et al. 1993; Bindeman and Valley 2001). Elders et al. (2011) compared the oxygen and hydrogen isotope composition of the Melt-1 glass to local groundwater, geothermal fluid, and hydrothermal epidote from Krafla. Present-day geothermal fluid shows some enrichment in $\delta^{18}O$ relative to local meteoric water due to exchange with volcanic rocks, but projects back to a local meteoric water source with $\delta^{18}O \sim -12.5$ ‰ and $\delta D \sim -90$ ‰ (Sveinbjörnsdóttir et al. 1986). The Melt-1 glass has lower δD (-121 ± 2 ‰; Elders et al. 2011) with values that directly overlap those of hydrothermal epidote recovered from several hydrothermal wells in Krafla (Elders et al. 2011). Elders et al. (2011) argue that the water in the rhyolite glass is entirely derived

Author's personal copy

Table 3 Trace element data on glass determined by LA-ICP-MS (mg/kg)

Grain	Melt-1				Melt-2		NIST 610	NIST 610[a]
	1700A	1700D	28A	28B	1700B	1700C		
# of Spots analyzed	3	4	3	5	2	3	12	
Sc	7	8	8	7	16	13	439	455
Ti	2,046	2,129	2,112	2,085	3,846	2,833	545	452
Mn	414	493	490	406	1,471	1,473	399	444
Co	2	1	1	2	1	1	379	410
Zn	61	72	76	62	226	220	454	460
Rb	64	89	91	66	635	649	391	426
Sr	54	54	55	54	14	15	485	516
Y	60	86	85	57	437	403	463	462
Zr	362	440	443	350	1,009	957	422	448
Nb	29	42	41	29	342	344	442	430
Cs	1	1	1	1	8	8	351	366
Ba	425	568	587	440	311	323	419	452
La	37	51	52	36	265	252	450	440
Ce	73	102	104	74	572	530	440	453
Nd	35	49	50	35	239	226	428	430
Sm	8	11	11	8	52	48	445	453
Gd	9	12	12	8	55	51	447	449
Dy	10	14	15	10	71	65	455	437
Er	6	9	9	6	47	43	476	455
Yb	7	10	10	7	52	47	486	450
Pb	4	5	5	4	25	25	406	426
Th	7	9	10	7	51	44	496	457
U	2	2	3	2	12	10	449	462

[a] Preferred values for NIST 610 glass Jochum et al. 2011

by melting hydrothermally altered basalt while the oxygen isotope ratios of the glass indicate a mixture of hydrothermally altered basalt and mantle-derived basalt. Pope et al. (2009) and Pope et al. (in review) present further $\delta^{18}O$ and δD analysis of basaltic and rhyolitic rocks and drill cuttings from the Krafla area in support of the model of generation of Melt-1 rhyolite by partial melting of hydrothermally altered basaltic crust deep beneath the Krafla Caldera.

It is possibility that felsic rocks, with compositions similar to the host felsite, were remelted and remobilized to form the melt lens. This process would require a high degree of melting in order for the composition of melt to match that of the source rocks. The exsolution textures in the pyroxenes and the evidence for partial melting of the host felsite both indicate that Melt-1 was derived from deeper in the system and was recently intruded to its present level. Melt segregation may have occurred by the mechanism outlined by Gunnarsson et al. (1998), but the high silica content and the light stable isotope ratios are not consistent with simple, one-stage, fractional crystallization of a basaltic magma as the source of the melt. Our data favor an origin by small degrees of partial melting of hydrothermally altered basaltic rocks, as proposed by Jónasson (1994).

Temperature and pressure estimates

Electron microprobe analyses of augite-pigeonite pairs that coexist in individual Melt-1 glass cutting fragments were used to calculate crystallization temperatures using QUILF and the pyroxene geothermometer of Anderson et al. (1993). Two pairs from the cores of grains gave the highest temperatures (997 and 981 °C), four pairs from intermediate zones ranged from 918 to 933 °C, and four pairs from the rims of crystals ranged from 922 to 940 °C. The extensive development of exsolution textures (Fig. 3b, c) and overgrowths of augite on some pigeonites (Fig. 3d) suggest that the pyroxenes record changing conditions of crystallization as Melt-1 moved up from its extraction depth to its level of emplacement (here after referred to as the in situ conditions). The temperatures recorded from the rims of pyroxenes likely represent the maximum in situ temperature of the melt. The pyroxene temperatures are

Author's personal copy

Table 4 Volatile content of Melt-1 glass determined by FTIR

Sample	H_2O mol	OH	H_2O 3570	H_2O total	H_2O 1 s error	CO_2 PPM	CO_2 1 s error	Saturation pressure (MPa)	T °C
Vesiculated									
28 I-1	0.54	1.16	n.d.	1.71	0.15	83	11	38.4	796
28 I-2	0.61	1.08	n.d.	1.69	0.14	72	10	36.2	796
Non vesiculated									
28 A-1	0.55	1.28	n.d.	1.83	0.12	97	13	44.2	916
28 A-2	0.54	1.23	n.d.	1.77	0.11	100	14	42.7	893
28 E-1	0.53	1.30	n.d.	1.84	0.13	114	14	48.6	939
28 E-2	0.49	1.24	n.d.	1.73	0.15			25.9	927
28 E-3	0.55	1.22	n.d.	1.77	0.15	92	12	41.6	883
2104 B-1	0.58	1.16	n.d.	1.74	0.15	78	10	38.5	845
2104 B-2	0.45	1.02	n.d.	1.47	0.13	77	10	31.3	836
2104 C-3	0.63	1.08	n.d.	1.70	0.14	69	10	36.0	788
2104 C-4	0.71	1.25	n.d.	1.96	0.18	75	11	44.4	839
2104 C-5	0.63	1.08	n.d.	1.71	0.15	65	9	35.6	789
2104 D-1	0.74	1.08	1.9	1.82	0.36	99	35	44.3	758
2104 D-2	0.84	1.25	1.6	2.09	0.31			36.7	800

H_2O mol molecular water as analyzed (5,300 cm^{-1}), *OH* hydroxyl as analyzed (4500 cm^{-1}), *H_2O 3570* total water as analyzed (3,570 cm^{-1}), only measurable on very thin samples, *H_2O total*: sum of H_2O mol and OH, *CO_2 (PPM)* concentration calculated with 2,350 cm^{-1} peak, *T* equilibration temperature using equation 8 of Ihinger et al. (1999), *n.d.* not detected

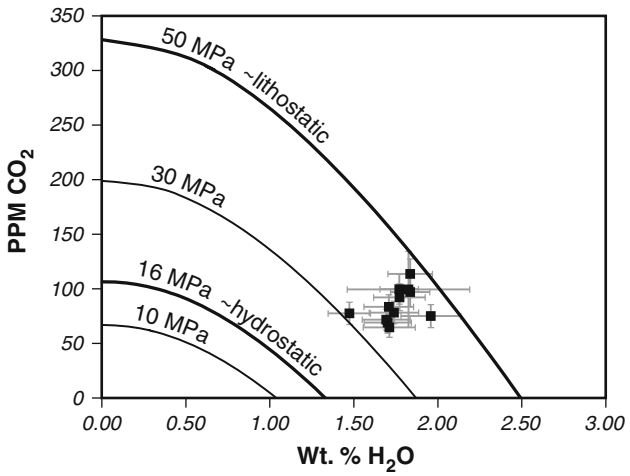

Fig. 8 Plot of H_2O versus CO_2 in Melt-1 glass determined by FTIR. Saturation pressure contours calculated using VolatileCalc (Newman and Lowenstern 2002). Hot hydrostatic pressure controlled by the depth to boiling curve is approximately 16 MPa; lithostatic pressure is approximately 50 MPa at the depth of emplacement (~2,100 m)

similar to pyroxene temperatures presented by Jónasson (1994) for rhyolites that have erupted at Krafla. Mafic cuttings recovered with the Melt-1 rhyolite glass are recrystallizing into granoblastic, pyroxene hornfels. Clinopyroxene–orthopyroxene–plagioclase–magnetite–ilmenite metamorphic assemblages in these cuttings also record temperatures in the range of 800–950 °C (Schiffman et al. in review).

Zoning in plagioclase crystals also records changing crystallization conditions. However, reversals in the plagioclase zoning indicate that the crystals are responding to changes other than the approximately 100 °C drop in temperature recorded by the pyroxenes as the melt ascended. Periodic loss of volatiles, particularly H_2O, will also affect the composition of growing plagioclase phenocrysts (Lange et al. 2009). Application of the Lange et al. (2009) model to plagioclase crystals in contact with Melt-1 glass, assuming measured water content of 1.77 wt%, gives temperatures of ~1,075–1,100 °C. These temperatures are likely too high for the in situ temperature because the melt was gas saturated and may have lost water during ascent its present depth (Elders et al. 2011). The plagioclase likely crystallized at temperatures lower than calculated, but at higher water contents and at greater depth, as the melt lost water during ascent. Re-equilibration of the plagioclase rim compositions with the melt by diffusive exchange following degassing would likely be very slow for these silicic melts. We can estimate the water content of a melt in equilibrium with An_{46} plagioclase by constraining the temperature. If we assume the plagioclase crystallized at the temperature calculated from pyroxene core compositions, 1,000 °C, the melt would require a water content of 2.9 wt% to match the existing plagioclase rim composition (Lange et al. 2009). A melt with 2.9 wt% H_2O at 1,000 °C requires pressures in excess of 90 MPa in order to avoid volatile-oversaturation (Newman and Lowenstern 2002), assuming the measured CO_2 concentration of 85 ppm

Author's personal copy

Table 5 Pyroxene compositions (wt %) determined by electron microprobe and calculated two-pyroxene temperatures (Anderson et al. 1993)

Sample-grain.spot	SiO_2	Al_2O_3	TiO_2	FeO	MnO	MgO	CaO	Na_2O	Total
Augite in Melt-1 glass									
28-R1.1	50.48	0.94	0.31	19.54	0.69	10.29	17.23	0.19	99.67
28-R3.1	50.87	1.02	0.36	19.52	0.66	10.53	17.33	0.19	100.48
28-R3.2	50.85	1.18	0.33	17.72	0.64	11.25	18.00	0.21	100.18
28-R3.3	50.90	1.06	0.31	18.14	0.64	11.12	17.90	0.20	100.27
28-R3.4	50.39	1.00	0.33	19.29	0.62	10.26	17.73	0.22	99.84
28-R3.5	50.06	1.13	0.38	20.51	0.71	9.48	17.63	0.23	100.13
28-R3.6	49.78	1.13	0.38	20.63	0.73	9.29	17.45	0.22	99.61
28-R3.7	49.80	1.17	0.41	21.14	0.70	8.88	17.64	0.18	99.92
28-R3.8	49.97	1.08	0.39	20.65	0.78	9.55	17.04	0.21	99.67
28-R3.9	50.39	1.01	0.31	19.23	0.65	10.53	17.00	0.18	99.30
28-R3.10	50.54	1.02	0.34	19.45	0.69	10.73	17.15	0.19	100.11
1700-R1.1	50.17	0.86	0.24	22.19	0.91	9.07	16.66	0.19	100.29
1700-R2.1	50.05	0.83	0.28	26.43	1.04	10.35	11.29	0.15	100.42
1700-R11.1	50.41	0.89	0.31	20.61	0.82	9.57	17.31	0.21	100.13
1700-R11.2	50.45	0.75	0.28	23.22	0.88	9.98	15.42	0.19	101.17
1700-R11.3	50.51	0.95	0.32	20.37	0.72	9.46	18.02	0.23	100.58
1700-R11.4	50.16	0.81	0.28	24.42	0.99	10.11	13.37	0.18	100.32
1700-R11.5	50.19	0.98	0.30	20.92	0.91	9.39	16.92	0.22	99.83
Average	50.36	1.01	0.33	20.20	0.73	9.96	17.28	0.20	100.07
Standard deviation	0.34	0.11	0.04	1.34	0.09	0.71	0.62	0.02	0.43
Pigeonite in Melt-1 glass									
28-R2.1	50.43	0.47	0.19	31.64	1.15	12.81	3.99	0.04	100.72
28-R4.1	50.11	0.45	0.19	31.40	1.17	12.90	3.93	0.04	100.19
28-4.2	50.20	0.55	0.19	29.45	1.10	12.53	5.83	0.05	99.90
28-R4.3	50.40	0.48	0.17	30.64	1.14	13.11	4.66	0.05	100.65
28-R4.4	50.39	0.48	0.15	31.36	1.14	12.99	4.12	0.03	100.66
28-R4.5	50.39	0.47	0.19	31.59	1.13	13.15	4.04	0.06	101.02
28-R4.6	50.09	0.47	0.20	31.31	1.23	13.14	4.10	0.06	100.60
28-R4.7	50.59	0.45	0.18	31.07	1.23	13.28	3.92	0.02	100.74
28-4.8	50.54	0.61	0.20	29.37	1.16	12.83	6.42	0.08	101.21
28-R4.9	50.18	0.45	0.20	31.75	1.17	13.03	4.07	0.06	100.91
28-R4.10	50.00	0.46	0.21	31.37	1.18	12.71	4.16	0.06	100.15
1700-R3.1	49.98	0.52	0.21	31.06	1.21	12.45	4.76	0.05	100.24
1700-R4.1	49.39	0.42	0.18	34.05	1.39	11.11	3.83	0.04	100.41
1700-R10.1	49.50	0.41	0.17	33.44	1.38	11.15	3.97	0.04	100.06
1700-R10.2	49.92	0.43	0.19	33.16	1.19	11.76	4.04	0.02	100.71
1700-R10.3	50.14	0.48	0.23	32.86	1.19	11.80	4.11	0.05	100.86
1700-R10.4	49.93	0.48	0.21	32.39	1.24	11.33	4.47	0.05	100.10
1700-R11.6	50.16	0.54	0.21	30.85	1.20	10.53	7.77	0.11	101.37
Average	50.10	0.46	0.19	31.94	1.21	12.45	4.14	0.04	100.53
Standard deviation	0.32	0.03	0.02	0.97	0.08	0.76	0.26	0.01	0.31
Augite in Melt-2-bearing felsite									
28-G5.1	50.22	0.84	0.18	19.88	1.47	7.04	20.33	0.55	100.51
28-G5.2	49.96	0.78	0.10	20.35	1.28	6.54	20.62	0.51	100.14
28-G5.3	49.54	0.77	0.10	21.39	1.36	6.08	20.42	0.56	100.22
28-G5.4	49.38	0.64	0.07	22.88	1.43	5.04	20.27	0.56	100.27
28-G6.1	50.35	0.83	0.20	18.67	1.21	7.59	20.84	0.58	100.27
28-G6.2	49.59	0.74	0.14	21.26	1.33	6.00	20.26	0.56	99.88

Author's personal copy

Table 5 continued

Sample-grain.spot	SiO_2	Al_2O_3	TiO_2	FeO	MnO	MgO	CaO	Na_2O	Total
28-G6.3	49.74	0.63	0.18	20.69	1.39	6.41	20.36	0.57	99.97
28-G6.4	49.86	0.67	0.19	20.27	1.47	6.79	20.55	0.56	100.36
28-G7.1	50.78	0.91	0.22	18.17	1.48	7.86	20.28	0.54	100.24
28-G7.2	49.62	0.78	0.12	19.94	1.36	6.64	20.20	0.55	99.21
28-G8.1	54.73	2.98	0.21	16.40	1.23	6.58	17.17	0.60	99.90
28-G8.2	50.17	0.82	0.22	19.25	1.42	7.13	20.20	0.55	99.76
28-G9.1	50.56	0.82	0.22	19.26	1.42	7.48	20.42	0.52	100.70
28-G9.2	50.04	0.80	0.15	20.91	1.55	6.36	20.13	0.58	100.52
28-G9.3	49.79	0.63	0.15	21.65	1.52	5.77	20.01	0.58	100.10
28-G9.4	50.35	0.81	0.19	20.21	1.43	6.98	20.25	0.61	100.83
1700-G12.1	50.38	0.73	0.16	19.49	1.57	7.62	20.04	0.57	100.56
1700-G12.2	49.98	0.74	0.21	18.83	1.38	7.76	20.29	0.53	99.72
1700-G12.3	50.58	0.73	0.17	18.63	1.53	7.93	20.23	0.57	100.37
1700-G12.4	50.47	0.74	0.17	18.41	1.63	8.12	20.47	0.53	100.54
1700-G12.5	50.65	0.72	0.20	18.48	1.62	8.18	20.49	0.55	100.89
1700-G13.1	50.56	0.75	0.20	18.45	1.65	8.12	20.11	0.51	100.35
1700-G13.2	50.73	0.77	0.21	18.12	1.72	8.37	20.31	0.57	100.80
1700-G13.3	50.91	0.79	0.21	18.15	1.72	8.38	20.38	0.53	101.07
1700-G13.4	50.99	0.78	0.23	18.31	1.60	8.35	20.21	0.55	101.02
1700-G14.1	48.84	1.09	0.41	23.94	1.54	5.08	18.89	0.50	100.29
1700-G14.2	49.30	1.08	0.42	22.28	1.55	6.28	19.18	0.52	100.61
1700-G14.3	51.04	0.87	0.23	18.55	1.42	8.00	19.93	0.51	100.55
Average	50.33	0.87	0.20	19.74	1.47	7.09	20.10	0.55	100.34
Standard deviation	1.01	0.42	0.07	1.66	0.13	0.97	0.68	0.03	0.41

Augite	Pigeonite	T°C (±)	Location
Two-pyroxene temperatures			
28-R1.1	28-R2.1	939 (53)	
28-R3.1	28-R4.1	938 (54)	Rim
28-R3.1	28-R4.10	940 (64)	Rim
28-R3.5	28-R4.5	981 (43)	Core
28-R3.6	28-R4.6	997 (74)	Core
28-R3.10	28-R4.1	922 (96)	Rim
28-R3.10	28-R4.10	922 (108)	Rim
1700-R1.1	1700-R4.1	933 (64)	
1700-R11.5	1700-R10.1	918 (77)	
1700-R11.1	1700-R10.4	921 (82)	

(Table 4). Any additional loss of CO_2 would imply that the starting pressure was greater than 90 MPa. This pressure implies the melt rose from a minimum depth of 3.6 km, assuming lithostatic pressure and an average density of 2,500 kg/m^3 for the overlying rock column.

The present in situ temperature of the melt is not well constrained. We used the Rhyolite-MELTS program (Gualda et al. 2012) in an attempt to model the crystallization of the melt. Our model input was the average composition of Melt-1 glass (Table 1) (i.e., we do not account for the ~3 % phenocrysts present in the glass), and the measured water content (1.77 wt%). The model predicts that plagioclase first crystallizes at 895 °C, followed by titanomagnetite at 890 °C, quartz at 885 °C, and orthopyroxene at 850 °C. The melt is 40 % crystallized by 845 °C and more than 95 % crystallized by 820 °C. The phenocrysts observed are augite and pigeonite, as opposed to the predicted orthopyroxene, and there are no quartz phenocrysts. Nevertheless, the in situ temperature of the melt is likely bracketed by the calculated pyroxene rim

Author's personal copy

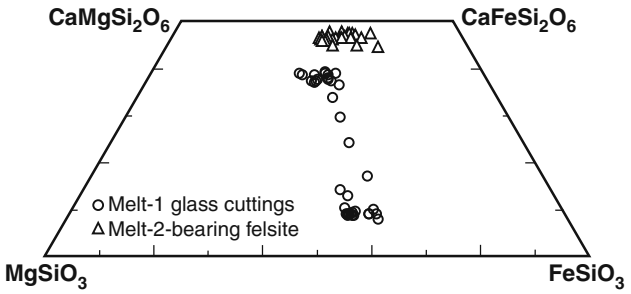

Fig. 9 Pyroxene quadrilateral showing compositions of augite and pigeonite phenocrysts in Melt-1 glass cuttings (*circles*). Points that plot between the augite and pigeonite fields likely overlap finely intergrown exsolution lamellae. Augites in Melt-2-bearing felsite cuttings (*triangles*) are shifted to more calcic compositions during partial melting of the felsite

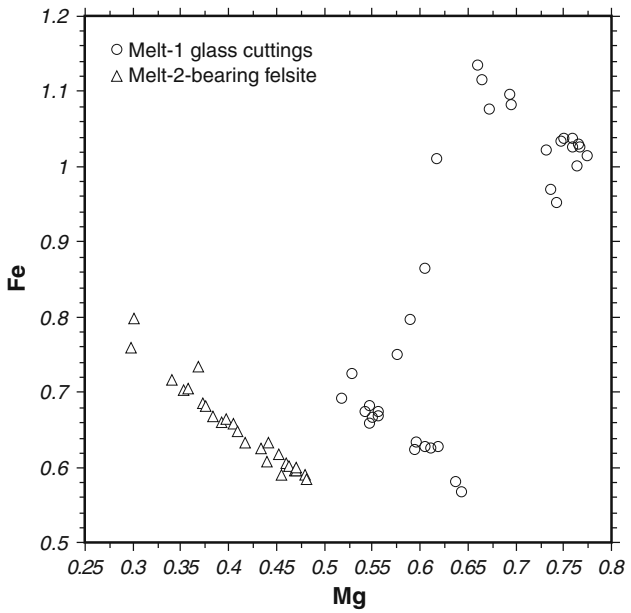

Fig. 10 Plot of Mg versus Fe in pyroxene in Melt-1 glass cuttings (*circles*) and Melt-2-bearing felsite cuttings (*triangles*)

temperature (~920 °C) and the temperature at which the Rhyolite-MELTS (Gualda et al. 2012) model predicts extensive crystallization of the melt (~850 °C).

Volatile measurements on the quenched Melt-1 glass provide some constraints on the in situ pressure (Table 4, Fig. 8). Although some glass fragments vesiculated prior to quenching (Fig. 2a,b), they have volatile contents that are identical to the more common, poorly vesiculated glass. Moreover, the presence of vesicles in both glass types clearly shows that degassing was ongoing and the melt was volatile-saturated. Plausibly, the glasses could be somewhat oversaturated if diffusion could not keep up with the pressure change, but the similarity in dissolved volatiles between the pumiceous and the poorly vesiculated samples is consistent with near-equilibrium degassing, and we conclude that the quenched glasses faithfully record the in situ volatile contents and the associated pressures. The high ratio of OH to H_2O in the glass (Table 4) is indicative of high temperature at which the melt was quenched to glass by the drilling fluid. Using the model of Ihinger et al. (1999), quenching temperatures between 760 and 940 °C are calculated. Saturation pressures calculated using VolatileCalc (Newman and Lowenstern 2002) assuming a temperature of 900 °C are mostly between 35 and 45 MPa. These pressures are below lithostatic pressure at the depth of emplacement (~50–57 MPa assuming densities of 2,500–2,700 kg/m^3) but are greater than the hot hydrostatic pressure of ~16 MPa of a boiling hydrothermal system (Fig. 8).

Maintaining pressures above the hot hydrostatic pressure in an active geothermal field suggests there must be a low permeability barrier that separates the melt lens from the overlying convective hydrothermal system. Loss of drill-water circulation immediately above the melt lens suggests there is a high permeability zone above the intrusion, but this zone is likely filled with superheated, dry steam.

Fluid circulation and cuttings returns reinitiated when cold drilling water interacted with the magma, resulting in subsurface steam explosions recorded as pressure pulses at the drill rig floor. A blanket of superheated steam adjacent to the melt lens may also explain the observation that cuttings collected 30–70 m above the melt show no hydrothermal alteration despite the high temperature (Schiffman et al. in review). The thermal boundary layer between the magma and the hydrothermal system will be controlled by the thermal conductivity of the chilled margin of the intrusion. The rate of convective heat transfer to the overlying active geothermal system would be controlled by the temperature and thickness of the steam blanket. The thickness of this potential steam blanket is poorly constrained at present, but preliminary flow test of the well produced superheated dry steam at 450 °C measured at the wellhead (G.Ó. Fridleifsson personal communication). While the temperature is well above the critical temperature of pure water, the pressure is lower than the critical point pressure.

Assimilation

Multiple intrusions of rhyolite melt into rhyolitic wall rocks is commonplace, but geologic evidence for the nature of this interaction is difficult to recognize in slowly cooled intrusives. The IDDP drill hole provides the first opportunity to study this interaction in detail because the circulation of drilling water quenched the various glasses, preserving their compositional differences. Despite the fact that the rhyolite magma (Melt-1) is nearly identical in

Author's personal copy

Table 6 Feldspar compositions (wt %) determined by electron microprobe

Sample-Grain.Spot	Na_2O	K_2O	CaO	BaO	Al_2O_3	Fe_2O_3	SiO_2	Total	An #	Ab	An	Or
Plagioclase in Melt-1 glass												
7-A1	6.16	0.30	8.83	n.a.	26.96	0.61	58.05	100.91	0.44			
7-A2	6.06	0.32	9.00	n.a.	26.98	0.58	57.64	100.57	0.45			
7-A3	6.27	0.32	8.85	n.a.	26.56	0.68	58.20	100.88	0.44			
7-A4	5.86	0.28	9.44	n.a.	27.30	0.72	56.92	100.53	0.47			
7-A5	5.85	0.26	9.37	n.a.	27.21	0.67	56.70	100.07	0.47			
7-E1	5.78	0.28	9.49	n.a.	27.07	0.58	57.02	100.22	0.48			
7-E2	5.80	0.30	9.15	n.a.	26.76	0.61	57.45	100.07	0.47			
7-E3	6.07	0.29	9.09	n.a.	26.97	0.62	57.58	100.61	0.45			
7-E4	6.11	0.31	8.92	n.a.	26.74	0.69	57.81	100.58	0.45			
7-HH1	5.75	0.26	9.64	n.a.	27.46	0.66	56.99	100.75	0.48			
7-HH2	5.56	0.25	10.14	n.a.	27.96	0.63	56.40	100.95	0.50			
7-HH3	5.70	0.25	9.72	n.a.	27.68	0.54	56.74	100.63	0.49			
7-HH4	6.67	0.31	8.07	n.a.	25.90	0.57	58.90	100.41	0.40			
28-R1	6.05	0.30	9.24	0.12	26.66	0.88	57.19	100.45	0.46			
28-R2	6.04	0.29	9.39	n.d.	27.23	0.86	56.72	100.53	0.46			
28-R3	5.98	0.30	9.61	n.d.	27.05	0.64	57.15	100.73	0.47			
28-R4	5.99	0.31	9.28	0.04	26.92	0.69	57.56	100.78	0.46			
28-R5	5.97	0.28	9.11	0.04	27.15	0.64	57.01	100.21	0.46			
28-R6	6.37	0.35	8.61	n.d.	26.17	0.64	58.41	100.55	0.43			
28-R7	6.15	0.32	8.92	n.d.	26.71	0.72	57.88	100.70	0.45			
28-R8	6.17	0.28	9.41	0.08	26.90	0.58	57.48	100.90	0.46			
1700-R1.1	6.31	0.35	8.62	0.13	26.61	0.61	57.72	100.35	0.43			
1700-R1.2	6.45	0.34	8.67	n.d.	26.50	0.55	57.54	100.05	0.43			
1700-R1.3	6.19	0.34	8.77	n.d.	26.65	0.62	57.51	100.08	0.44			
1700-R2.1	6.23	0.31	8.71	0.04	26.78	0.57	57.87	100.51	0.44			
1700-R2.2	6.38	0.35	8.60	0.13	26.77	0.54	58.29	101.05	0.43			
1700-R2.3	6.27	0.35	8.58	n.d.	26.81	0.67	58.17	100.86	0.43			
Plagioclase in Melt-2-bearing felsite												
28-G1	6.21	0.56	8.41	n.d.	26.81	0.65	57.48	100.11	0.43			
28-G2	6.54	0.59	8.27	0.09	26.75	0.65	57.69	100.58	0.41			
28-G3	6.27	0.56	8.80	0.12	26.91	0.60	57.24	100.50	0.44			
28-G4	6.15	0.53	8.97	n.d.	27.18	0.60	56.85	100.29	0.45			
Alkali feldspar in Melt-2-bearing felsite												
7-K.1	7.34	4.95	1.34	n.a.	19.85	0.55	66.27	100.30		0.65	0.07	0.29
7-K.2	7.34	4.54	1.48	n.a.	20.18	0.53	66.22	100.28		0.66	0.07	0.27
7-K.3	7.09	5.26	1.16	n.a.	20.01	0.42	66.53	100.47		0.63	0.06	0.31
7-K.4	7.48	4.77	1.47	n.a.	20.05	0.47	66.27	100.52		0.65	0.07	0.27
7-K.5	7.47	4.47	1.62	n.a.	20.30	0.50	65.98	100.34		0.66	0.08	0.26
7-K.6	7.11	5.38	1.25	n.a.	20.20	0.13	65.96	100.03		0.63	0.06	0.31
28-G1	7.59	4.30	1.68	0.15	20.29	0.50	65.88	100.39		0.67	0.08	0.25
28-G2	7.67	4.34	1.71	0.04	20.76	0.55	65.54	100.61		0.67	0.08	0.25
28-G3	7.53	4.35	1.80	0.11	20.55	0.41	65.81	100.54		0.66	0.09	0.25
1700-G1.1	7.64	3.76	2.11	0.09	20.57	0.54	64.52	99.24		0.68	0.10	0.22
1700-G1.2	7.72	4.40	1.57	0.21	20.58	0.58	65.87	100.94		0.67	0.08	0.25
1700-G1.3	7.15	4.43	1.53	0.17	19.57	0.65	66.70	100.21		0.65	0.08	0.27
1700-G2.1	7.66	4.27	1.69	n.a.	20.25	0.49	66.09	100.46		0.67	0.08	0.25
1700-G2.2	7.79	3.71	2.27	n.a.	20.69	0.46	65.46	100.38		0.68	0.11	0.21

Author's personal copy

Table 6 continued

Sample-Grain.Spot	Na_2O	K_2O	CaO	BaO	Al_2O_3	Fe_2O_3	SiO_2	Total	An #	Ab	An	Or
1700-G2.3	7.59	4.18	1.90	n.a.	20.70	0.52	65.67	100.55		0.67	0.09	0.24
1700-G2.4	7.53	4.58	1.52	n.a.	20.17	0.44	66.27	100.51		0.66	0.07	0.26
Ternary feldspar in Melt-2-bearing felsite												
1700-G1.1	8.13	1.79	4.14	n.d.	22.98	0.24	63.65	100.92		0.70	0.20	0.10
1700-G1.2	8.07	1.56	4.41	0.09	23.34	0.29	63.00	100.76		0.70	0.21	0.09
1700-G1.3	8.08	1.73	4.01	0.07	23.21	0.22	63.44	100.76		0.71	0.19	0.10
Plagioclase in Melt-3 glass												
7-CC1	6.60	0.46	7.94	n.a.	26.15	0.65	58.82	100.61	0.40			
7-CC2	6.77	0.49	7.94	n.a.	26.02	0.57	58.72	100.51	0.39			
7-CC3	6.11	0.42	8.73	n.a.	26.91	0.58	58.02	100.77	0.44			
7-CC4	7.47	0.68	6.39	n.a.	24.61	0.54	60.51	100.20	0.32			
7-CC5	6.11	0.40	9.02	n.a.	27.04	0.73	57.32	100.62	0.45			
1700-ZP1	6.71	0.49	7.51	n.a.	25.84	0.55	59.51	100.61	0.38			
1700-ZP2	5.82	0.34	9.77	n.a.	27.93	0.63	56.29	100.78	0.48			
1700-ZP3	4.66	0.19	11.74	n.a.	29.38	0.72	53.97	100.65	0.58			
1700-ZP4	5.82	0.28	9.59	n.a.	27.61	0.49	56.65	100.45	0.48			
1700-ZP5	5.17	0.21	10.75	n.a.	28.53	0.43	55.46	100.56	0.53			

n.a. not analyzed, *n.d.* not detected

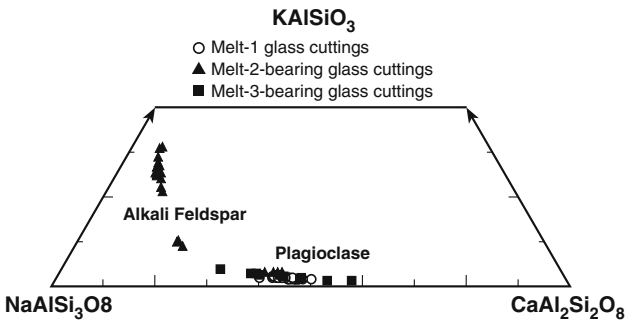

Fig. 11 Feldspar compositions in Melt-1 glass cuttings (*circles*), Melt-2-bearing felsite cuttings (*triangles*) and glomerocrysts in Melt-3 glass cuttings (*squares*)

composition to the felsite wall rocks, the melt has sufficient heat content to induce partial melting in the host rocks, forming interstitial pockets of Melt-2. It is difficult to quantify the extent of partial melting from the cuttings, but examination under the binocular microscope or using the BSE images (Fig. 4a) suggests that proportion of melt is small, on the order of 10 %. The partial melt (Melt-2) is enriched in K and depleted in Ca relative to the whole-rock compositions and matches well with low-pressure melting experiments in granite system (Tuttle and Bowen 1958; Luth et al. 1964). Incompatible elements are strongly partitioned into the melt with LIL ions showing the strongest enrichment (Fig. 7b). Exceptions to the general pattern of decreasing incompatibility with increasing charge to cation ratio are Ba and Sr, elements that freely substitute for Ca in plagioclase.

Unequivocal textural evidence for assimilation of felsite by the rhyolite melt (Fig. 4b,d) is complimented by the chemical analysis of the quenched Melt-3 glass, which occurs in the rare crystal-rich, glomeroporphyritic cuttings. On compositional co-variation plots involving K_2O, Na_2O, CaO, MgO, and FeO (e.g., Fig. 6a, b), the glomeroporphyritic, assimilated samples always plot between the composition of Melt-1 and Melt-2, consistent with an origin by simple mixing of these end-member melts. However, variation diagrams including SiO_2 indicate the addition of silica to the Melt-3 glass, presumably due to quartz dissolution. The trend of increasing K_2O and decreasing CaO with increasing SiO_2 (Fig. 6c, d) in the Melt-1 glass suggests fractionation by plagioclase crystallization, which is supported by the decrease in Al_2O_3 with increasing SiO_2. Continued growth of augite also likely contributed to the CaO decrease, as both MgO and FeO show similar trends. These differentiation trends are not apparent in the Melt-2 glass with the exception of K_2O, which decreases with increasing SiO_2 (Fig. 6c), consistent with textural evidence for resorption of both quartz and alkali feldspar.

Composite intrusive suites formed by multiple emplacement of compositionally similar sills, similar to what is occurring at Krafla, have been described elsewhere (e.g., Walker et al. 2007). The compositional variations in the glasses are relatively minor and would be very difficult to recognize if these rocks had continued to cool slowly underground until they crystallized. It is interesting to speculate about our ability to recognize the interaction of a

Author's personal copy

felsic melt with felsic wall rocks in a crystallized sequence of intrusives. The results of this study suggest three possible lines of evidence that could be used to unravel such processes in older intrusive sequences. The first is the textural evidence for resorption of quartz and alkali feldspar. Both the partially melted felsites and the assimilated felsite are characterized by subhedral to rounded crystals of titanomagnetite, pyroxene, and plagioclase compared with the phenocrysts in the rhyolite (Melt-1), but the textural evidence in completely crystalline rocks would be less definitive. However, the glomeroporphyritic nature of the partially assimilated felsite (Melt-3) would be more likely to survive. A more definitive signal of partial melting and assimilation would likely be preserved in the composition of the augites. The augite evolves to more calcic compositions (Fig. 9a) during the partial melting and is very similar to metamorphic clinopyroxene found in basaltic rocks thermally metamorphosed by the rhyolite intrusion (Schiffman et al. in review). The augites in the partially melted felsite also have higher contents of Mn and Na compared with augite phenocrysts in the rhyolite melt (Melt-1). Finally, the patches of partial melt will eventually crystallize to a mineral assemblage that is similar to the host rock, although perhaps finer-grained and depleted in mafic phases. While these may be difficult to recognize texturally, the strong enrichment in incompatible elements, coupled with the low diffusion rates of silicic melts, suggests that these former melt pocket should be distinguishable due to the compositional heterogeneity of the crystalline rocks. Similar processes may also contribute to compositional zoning of REEs observed in zircons that record extended growth in composite batholiths (Claiborne et al. 2010).

Conclusions

Results of IDDP drilling in the Krafla geothermal field capture textural and geochemical evidence for the recent emplacement of a sparsely phyric, relatively anhydrous, high-silica rhyolite melt lens into crystalline rocks of nearly identical composition. The rhyolite melt originated by partial melting of crustal rock that was hydrothermally altered by isotopically light meteoric water. The melt began crystallizing plagioclase, augite, pigeonite, and titanomagnetite at temperatures near 1,000 °C during rise of the melt to its emplacement depth of 2,100 m. Pyroxene rim compositions suggest the melt has a maximum in situ temperature of approximately 920 °C; modeling using Rhyolite-MELTS suggests a minimum in situ temperature of approximately 850 °C. The melt has partially degassed at its present depth at pressures that are between lithostatic and hydrostatic. Heat from the intrusion has partially melted the wall rocks producing a melt near the low-pressure minimum in the granite system. Locally, the rhyolite melt has mixed with the incipient melt from the felsite and has partially assimilated its felsite wall rocks producing a glomerocryst-rich melt that has higher silica content than either of the end-member melts due to resorption of quartz. Processes such as partial melting of felsic host rock due to emplacement of rhyolite melt, magma mixing, and assimilation, which are easily distinguishable in this system due to our ability to analyze quenched glasses, must be commonplace in felsic intrusive suites, but these effects will be more difficult to recognize once the various melts have crystallized. However, careful petrographic investigation including mineral textures, coupled with in situ chemical analysis showing heterogeneous distribution of incompatible elements such as the REEs may be used as evidence of magma–wall rock interaction in crystalline rocks.

Acknowledgments This research would not have been possible without the generous cooperation of Landsvirkjun and the IDDP consortium. The work was supported by NSF grants EAR 0507518 and EAR 0506882. Reviews by Bruce Marsh, Christy Till and anonymous reviewers improved the manuscript.

References

Anderson DL, Lindsley DH, Davidson PM (1993) QUILF: a Pascal program to assess equilibria among Fe-Mg-Mn-Ti oxides, pyroxenes, olivine, and quartz. Comput Geosci 19:1333–1350

Ármannsson H (2010) IDDP: the chemistry of the Krafla geothermal system in relation to the IDDP well. In: Proceedings of the world geothermal congress 2010. Bali, Indonesia, 25–29 April, paper 3906, pp 1–5

Ármannsson H, Guðmundsson A, Steingrímsson BS (1987) Exploration and development of the Krafla geothermal area. Jökull Icel J Earth Sci 37:13–30

Ármannsson H, Benjamínsson J, Jefferies AWA (1989) Gas changes in the Krafla geothermal system, Iceland. Chem Geol 76:175–196

Arnórsson S, Axelsson G, Sæmundsson K (2008) Geothermal systems in Iceland. Jökull Icel J Earth Sci 58:269–302

Bindeman IN, Valley JN (2001) Low-δ^{18}O Rhyolites from Yellowstone: magmatic evolution based on analyses of zircons and individual phenocrysts. J Petrol 42:1491–1517

Böðvarsson GS, Pruess K, Steffánson V, Elíasson ET (1984) The Krafla geothermal field, Iceland. 2. The natural state of the system. Water Resour Res 20:1545–1559

Brophy JG (2009) La-SiO2 and Yb-SiO2 systmenatics in mid-ocean ridge magmas: implications for the origin of oceanic plagiogranite. Contrib Mineral Petrol 158:99–111

Claiborne LL, Miller CF, Wooden JL (2010) Trace element composition of igneous zircon: a thermal and compositional record of the accumulation and evolution of a large silicic batholith, Spirit Mountain, Nevada. Contrib Mineral Petrol 160:511–531

Condomines M, Grönvold K, Hooker P, Muehlenbachs K, O'Nions RK, Oskarsson N, Oxburgh R (1983) Helium, oxygen, strontium and neodymium isotopic relationships in Icelandic volcanics. Earth Planet Sci Lett 66:125–136

Author's personal copy

Eiler JM (2001) Oxygen isotope variation of basaltic lavas and upper mantle rocks. Rev Mineral Geochem 43:319–364

Einarsson P (1978) S-wave shadows in the Krafla caldera in NE Iceland, evidence for a magma chamber in the crust. Bull Volcanol 41:187–195

Einarsson K, Pálsson B, Gudmundsson Á, Hólmgeirsson S, Ingason K, Matthíasson J, Hauksson T, Ármannsson H (2010) Acid wells in the Krafla geothermal field. In: Proceedings of the world geothermal congress 2010. Bali, Indonesia, 25–29 April 2010, paper 2731, pp 1–6

Elders WA, Friðleifsson GÓ (2010) The science program of the Iceland deep drilling project (IDDP): a study of supercritical geothermal resources. In: Proceedings of the world geothermal congress. Bali Indonesia, 25–29 April 2010, pp 1–9

Elders WA, Friðleifsson GÓ, Zierenberg RA, Pope EC, Mortensen AK, Gudmundsson A, Lowenstern JB, Marks NE, Owens L, Bird DK, Reed M, Olsen NJ, Schiffman PA (2011) Origin of a rhyolite that intruded a geothermal well while drilling in a basaltic volcano, at Krafla, Iceland. Geology 39:231–234

France L, Koepke J, Ildefonse B, Cichy SB, Deschamps F (2010) Hydrous partial melting in the sheeted dike complex at fast spreading ridges: experimental and natural observations. Contrib Mineral Petrol 160:683–704

Friðleifsson GÓ, Elders WA (2005) The Iceland deep drilling project: a search for deep unconventional geothermal resources: Geotherm 34:269–285

Friðleifsson GÓ, Albertsson A, Elders WA (2010) Iceland deep drilling project (IDDP)—10 years later—still an opportunity of international collaboration. In: Proceedings of the world geothermal congress. Bali Indonesia, 25–29 April 2010, pp 1–5

Gautason B, Árnadóttir S, Mortensen AK, Egilson Þ, Guðfinnsson GH, Sigurgeirsson MÁ, Jónsson RB, Tryggvason H, Gunnarsson HS, Sveinbjörnsson S, Þorsteinsson E, Ingimarsdóttir A, Massiot C (2010) Krafla—IDDP-1. Drilling completion and geology report for drilling stage 4. Íslenskar orku-rannsóknir, ÍSOR-2010/116. Unnið fyrir Landsvirkjun, LV-2010/131

Gualda GAR, Ghiorso MS, Lemons RV, Carley TL (2012) Rhyolite-MELTS: a modified calibration of MELTS optimized for silica-rich, fluid-bearing magmatic systems. J Petrol 53:875–890

Guðmundsson Á (1983) The geology of the Krafla Suðurhlíðar field, in ravens congregation on the status of the Krafla geothermal power station, 2–3 March 1983, Krafla power station, Akureyri, Iceland, pp 77–85 (in Icelandic)

Guðmundsson Á, Steingrímsson B, Ármannsson H, Thórhallsson S (2008) An estimate of the state of well KJ-36, Krafla at the beginning of the year 2008. ÍSOR Memo, pp 1–3

Gunnarsson B, Marsh BD, Taylor HP Jr (1998) Generation of Icelandic rhyolites: silicic lavas from the Torfajökull central volcano. J Volc Ceotherm Res 83:1–45

Harmon RS, Hoefs J (1995) Oxygen isotope heterogeneity of the mantle deduced from global 18O systematics of basalts from different geotectonic settings. Cont Mineral Petrol 120:95–114

Hattori K, Muehlenbachs K (1982) Oxygen isotope ratios of the Icelandic crust. J Geophys Res 87:6559–6565

Hémond C, Arndt NT, Lichtenstein U, Hofmann AW, Oskarsson N, Steinthorsson S (1993) The heterogeneous Iceland plume: Nd-Sr-O isotopes and trace element constraints. J Geophys Res 98:15833–15850

Hólmgeirsson S, Guðmundsson Á, Pálsson B, Bóasson HA, Ingason K, Þórhallsson S (2010) Drilling operations of he first Iceland deep drilling well (IDDP). In: Proceedings of the world geothermal congress. Bali Indonesia, 25–29 April 2010, pp 1–10

Ihinger PD, Zhang Y, Stolper EM (1999) The speciation of dissolved water in rhyolitic melt. Geochimic Cosmochim Acta 63:3567–3578

Jochum KP, Weis U, Stoll B, Kuzmin D, Yang Q, Raczek I, Jacob DE, Stracke A, Birbaum K, Frick DA, Günther D, Enzweiler J (2011) Determination of reference values for NIST SRM 610–617 glasses following ISO guidelines. Geostandards Geoanalytical Res 35:397–429

Jónasson K (1994) Rhyolite volcanism in the Krafla central volcano, Northeast Iceland. Bull Volcanol 56:516–528

Jónasson K (2007) Silicic volcanism in Iceland: composition and distribution within the active volcanic zones. J Geodynam 43: 101–117

Kristmannsdóttir H (1978) Alteration of bedrock in the Krafla geothermal system. Report no. OS/JHD-7854, Orkustofun, Reykjavik, pp 1–29 (in Icelandic)

Lange RA, Frey HM, Hector J (2009) A thermodynamic model for the plagioclase-liquid hygrometer/thermometer. Am Mineral 94: 494–506

Lowenstern JB, Clynne MA, Bullen TD (1997) Comagmatic A-type granophyre and rhyolite from the Alid volcanic center, Eritrea, northeast Africa. J Petrol 38:1707–1721

Luth WC, Jahns RH, Tuttle OF (1964) The granite system at pressures of 4–10 kilobars. J Geophys Res 69:759–773

Marks N, Schiffman P, Zierenberg RA, Franzson H, Friðleifsson GÓ (2009) Hydrothermal alteration in the Reykjanes geothermal system: insights from Iceland deep drilling program well RN-17. J Volcanol Geotherm Res 189:172–190

Moorbath S, Walker GPL (1965) Strontium isotope investigation of igneous rocks from Iceland. Nature 207:837–840

Mortensen AK, Grönvold K, Gudmundsson Á, Steingrímsson BS, Egilson Þ (2010) Quenched silicic glass from well K-39 in Krafla, North-Eastern Iceland. In: Proceedings of the world geothermal congress 2010, Bali, Indonesia, 25–29 April 2010, Paper 1284, pp 1–6

Muehlenbachs K, Anderson AT Jr, Sigvaldason GE (1974) Low-O18 basalts from Iceland. Geochim Cosmochim Acta 38:577–588

Newman S, Lowenstern JB (2002) VolatileCalc: a silicate melt-H2O-CO2 solution model written in visual basic for excel. Comput Geosci 28:597–604

Nicholson H, Condomines M, Fitton GJ, Fallick AE, Grönvold K (1991) Assimilation beneath Krafla, Iceland. J Petrol 32:1005–1020

Pope EC, Bird DK, Arnórsson S, Fridriksson Þ, Elders WA, Friðleifsson GÓ (2009) The Iceland deep drilling project: stable isotope constraints of fluid source and evolution in Icelandic geothermal systems. Trans Geotherm Resour Counc 33:411–416

Pope EC, Bird DK, Arnórsson S (in review) Evolution of low-^{18}O Icelandic crust: perspectives from the IDDP-1 rhyolite melt. Geochim Cosmochim Acta

Rose-Koga EF, Sigmarsson O (2008) B-O-Th isotope systematics in Icelandic tephra. Chem Geol 255:454–462

Sæmundsson K (1978) Fissure swarms and central volcanoes of the neovolcanic zones of Iceland. Geol J Spec Issue 10:415–432

Sæmundsson K (1991) Geology of the Krafla system. In: Gardarsson A, Einarsson Á (eds) Náttúra Mývatns Hid Íslenska Náttúrufraedifélag, Raykjavík, pp 25–95 (in Icelandic)

Sæmundsson K (2008) Geological map of Krafla, 1: 25,000. Prepared for the national power company (Landsvikjun) and the Iceland GeoSurvey (ISOR), Reykjavik

Schiffman P, Zierenberg RA, Friðleifsson GÓ, Elders WA (in review) High temperature metamorphism in the conductive boundary layer adjacent to a rhyolite intrusion in the Krafla geothermal system. Gethermics

Sigmarsson O, Hémond C, Condomines M, Fourcade S, Oskarsson N (1991) Origin of silicic magma in Iceland revealed by Th isotopes. Geology 19:621–624

Sigmarsson O, Condomines M, Fourcade S (1992) Mantle and crustal contribution in the genesis of Recent basalts from off-rift zones

Author's personal copy

in Iceland. Constraints from Th, Sr, and O isotopes. Earth Planet Sci Lett 110:149–162

Skovgaard AC, Storey M, Baker J, Blusztajn J, Hart SR (2001) Osmium-oxygen isotopic evidence for a recycled and strongly depleted component in the Iceland mantle plume. Earth Planet Sci Lett 194:259–275

Spulber SD, Rutherford MJ (1983) The origin of rhyolite and plagiogranite in oceanic crust: an experimental study. J Petrol 24:1–25

Stefánsson V (1980) Investigation on the Krafla high temperature geothermal field. Náttúrufræðingurinn 50:333–359 (In Icelandic, English summary)

Stefánsson V (1981) The Krafla geothermal field, Northeast Iceland, chapter 10. In: Rybach L, Muffler LJP (eds) Geothermal systems: principles and case histories. John Wiley and Son Ltd, New York, pp 273–294

Sun SS, McDonough WF (1989) Chemical and isotopic systematics of ocean basalts: implications for mantle compositions and processes. In: Saunders AD, Norry MJ (eds) Magmatism in the Ocean Basins. Geol Soc London Spec Pub 42:313–345

Sveinbjörnsdóttir AE, Coleman ML, Yardley BWD (1986) Origin and history of hydrothermal fluids of the Reykjanes and Krafla geothermal fields, Iceland: a stable isotope study. Contrib Mineral Petrol 94:99–109

Teplow W, Marsh B, Hulen J, Spielman P, Kaleeikinin M, Fitch D, Rickard W (2009) Dacite Melt at the Puna geothermal venture well field, big Island of Hawaii. Geotherm Resour Counc Trans 33:989–994

Thirlwall MF, Gee MAM, Lowry D, Mattey DP, Murton BJ, Taylor RN (2006) Low $\delta^{18}O$ in the Icelandic mantle and its origins: evidence from Reykjanes Ridge and Icelandic lavas. Geochim Cosmochim Acta 70:993–1019

Thy P, Beard JS, Lofgren GE (1990) Experimental constraints on the origin of Icelandic rhyolites. J Geol 98:417–421

Tuttle OF, Bowen NL (1958) Origin of granite in light of experimental studies in the system $NaAlSi_3O_8$-$KAlSi_3O_8$-SiO_2-H_2O. Geol Soc Am Mem 74:1–153

Walker BA Jr, Miller CF, Claiborne LL, Wooden JL, Miller JS (2007) Geology and geochronology of the Spirit Mountain batholith, southern Nevada: implications for timescales and physical processes of batholith construction. J Volcanol Geothermal Res 167:239–262

Winter JD (2001) An introduction to igneous and metamorphic petrology. Prentice-Hall Inc, New Jersey